Available online at www.sciencedirect.com
SCIENCE DIRECT®
ELSEVIER
International Journal of Solids and Structures 43 (2006) 2602–2630
INTERNATIONAL JOURNAL OF SOLIDS and STRUCTURES
www.elsevier.com/locate/ijsolstr

Nonlinear transient response of strain rate dependent composite laminated plates using multiscale simulation

Linfa Zhu [a,*], Aditi Chattopadhyay [a], Robert K. Goldberg [b]

[a] *Department of Mechanical and Aerospace Engineering, Arizona State University, Tempe, AZ 85287-6106, USA*
[b] *National Aeronautics and Space Administration, Glenn Research Center, Cleveland, OH 44135, USA*

Received 17 January 2005; received in revised form 2 June 2005
Available online 2 August 2005

Abstract

The effects of strain rate dependency and inelasticity on the transient responses of composite laminated plates are investigated. A micromechanics model which accounts for the transverse shear stress effect, the effect of strain rate dependency and the effect of inelasticity is used for analyzing the mechanical responses of the fiber and matrix constituents. The accuracy of the micromechanics model under transverse shear loading is verified by comparing the results with those obtained using a general purpose finite element code. A higher order laminated plate theory is extended to capture the inelastic deformations of the composite plate and is implemented using the finite element technique. A complete micro–macro numerical procedure is developed to model the strain rate dependent behavior of inelastic composite laminates by implementing the micromechanics model into the finite element model. Parametric studies of the transient responses of composite plates are conduced. The effects of geometry, ply stacking sequence, material models, boundary conditions and loadings are investigated. The results show that the strain rate dependency and inelasticity influence the transient responses of composite plates via two significantly different mechanisms.

Keywords: Transient response; Composite laminates; Multiscale simulation; Micromechanics model

1. Introduction

Due to their light weight, excellent strength to weight ratio and energy absorption capability, heterogeneous materials such as fiber-reinforced and woven composites are increasingly being used in impact related

* Corresponding author. Tel.: +1 4807270007; fax: +1 4809651384.
E-mail address: linfa.zhu@asu.edu (L. Zhu).

0020-7683/$ - see front matter © 2005 Elsevier Ltd. All rights reserved.
doi:10.1016/j.ijsolstr.2005.06.033

applications. Currently, there is an effort to develop polymer matrix composite (PMC) fan-containment systems to reduce the weight and cost while maintaining the high levels of safety associated with current systems. The polymer composite in the engine containment system is very susceptible to projectile impact such as failed blades separating from the rotor during operation. Therefore, efficient design, test and analysis procedures are urgently needed for modeling the high-speed impact of composite materials. The types of polymer matrix composites that are used in such an application have a deformation response that is nonlinear and that varies with strain rate. Thus, it is important to develop a framework for simulating and predicting the deformation and failure behavior of polymer matrix composite structures subjected to impact loadings. The analysis methodology must be able to account for strain rate effects, material nonlinearities and transverse shear stresses, which are important in impact problems. The computational efficiency, which is critical in the micro–macro numerical analysis of such a problem, particularly when used in a design environment, must be considered. The objective of this work is to develop an efficient micro–macro numerical framework addressing the issues discussed above and to investigate their effects on the transient response of laminated composite plates.

Extensive reviews of various theories proposed for evaluating the characteristics of composite laminates, including the Laplace transform technique (Chow, 1971), the method of characteristics (Wang et al., 1972), equivalent single-layer laminate theories (Reddy, 1997) and 3-D finite element methods, can be found in Noor and Burton (1989), Kapania and Raciti (1989), Reddy (1990), Mallikarjuna and Kant (1993), and Varadan and Bhaskar (1997). Due to their computational efficiency and accuracy, equivalent single-layer laminate theories have been widely used for the macroscopic characterizations of composite laminates. As is well known, the classical laminated plate theory (CLPT) (Kant and Khare, 1994), which is an extension of classical plate theory (CPT) (Khdeir and Reddy, 1991; Khdeir et al., 1992), neglects the effects of transverse shear strains. Due to a high ratio of in-plane Young's moduli to transverse shear moduli for most composite laminates, the transverse shear deformations for a composite are more pronounced compared to those of isotropic plates. To address this issue, the first order shear deformation theory (FSDT) (Whitney, 1969), based on the work of Pao (1972) and Flugge (1967), assumes linear in-plane displacements through the laminate thickness. Using FSDT, the transient responses of rectangular composite plates have been investigated by Reddy (1982, 1983). Since constant transverse shear stresses are assumed, shear correction coefficients are needed to rectify the unrealistic variation of the shear strains and shear stresses through the thickness. In order to overcome these limitations, several higher order theories (HOTs) (Reddy, 1984; Chattopadhyay and Gu, 1994), assuming cubic through-the-thickness variations in displacements, have been developed. In HOTs, the conditions of zero transverse shear stresses on the top and bottom surfaces are imposed, eliminating the need for shear correction coefficients while maintaining computational efficiency. Kant and Mallikarjuna (1991), Kant et al. (1988), Kommineni and Kant (1993), Mallikarjuna and Kant (1990), Kant et al. (1990), Kant et al. (1992) investigated the linear and nonlinear transient responses of composite plates using a C^0 HOT finite element method. However, the effect of strain rate dependency of the composite material, which is essential in the impact problem, was not addressed.

The micromechanics approach has been applied to compute the deformation response of composites in which the material response is nonlinear. In micromechanics models, the overall properties and responses of the composites are computed based on the properties and responses of the individual constituents. Plasticity and viscoplasticity based constitutive equations can be used to compute the nonlinear response of the matrix constituent (assuming the fiber is linear elastic, as is usually the case for polymer matrix composites), and homogenization methods can then be applied to compute the overall (nonlinear) response of the composite. The methodology is based on defining a unit cell in the composite material. The behavior of the unit cell can be assumed to be equivalent to the response of a specific point in the composite laminate. Several variations of this approach have been reported. The method of cells (MOC) was developed by Aboudi (1989) for unidirectional fiber-reinforced composites with elasto-viscoplastic constituents. Pindera and

Bednarcyk (1999) reformulated the MOC using simplified uniform stress and strain assumptions, resulting in considerably improved computational efficiency. By applying a similar approach and discretizing the composite unit cell into three subcells, a two-dimensional elastic–plastic model was developed by Sun and Chen (1991). This model was then extended to three dimensions by Robertson and Mall (1993). A more precise elastic micromechanics model was proposed by Whitney (1993) where the unit cell was divided into an arbitrary number of rectangular, horizontal slices. Mital et al. (1995) used a slicing approach to compute the effective elastic constants and microstresses (fiber and matrix stresses) in ceramic matrix composites. In this work, a mechanics of materials approach was used to compute the effective elastic constants and microstresses in each slice of a unit cell. Laminate theory was then applied to obtain the effective elastic constants for the unit cell as well as the effective stresses in each slice. Goldberg et al. (2003, 2004), Goldberg (2000) extended this slicing approach to include the material nonlinearity and strain rate dependency in the deformation analysis of carbon fiber-reinforced polymer matrix composites, and this advanced micromechanics model was implemented into CLPT for the analyses of symmetric thin laminated plates subject to in-plane loading. Kim et al. (2004) incorporated the effect of transverse shear stresses into this model and implemented it into a refined HOT to investigate the constitutive relationship of the laminated plate when loaded at various strain rates.

In this paper, the effects of strain rate dependency and inelasticity on the transient responses of composite laminated plates are investigated using a micro–macro numerical procedure. Firstly, the inelastic constitutive model used to model the nonlinear, strain rate dependent deformations of the polymer matrix constituent, and the previously developed micromechanics model which considers the effects of transverse shear stresses, strain rate dependency and material inelasticity are briefly described. The accuracy of the micromechanics model under transverse shear loading is verified by comparing the results with those obtained using the commercial finite element code ABAQUS/Explicit (Anonymous, 2003). Next, the implementation of the micromechanics model into a nonlinear HOT based finite element model, in order to improve the ability of the methodology to analyze polymer matrix composites subjected to impact loadings, is presented. Finally, parametric studies of the transient responses of composite laminated plates with various geometries and stacking sequences, using various material models, under various boundary conditions and subjected to suddenly applied loadings of various magnitudes, are addressed. It is expected that the results obtained from this procedure can be used to provide optimum design guidelines for composite laminated plates subject to impact loadings.

2. Nonlinear micromechanics model

A brief description of the nonlinear micromechanics model is presented. The model includes strain rate dependency, inelastic material behavior and the effect of transverse shear stresses. More detailed information can be found in Goldberg et al. (2003, 2004), Goldberg (2000), Kim et al. (2004).

2.1. Constitutive equations to analyze nonlinear deformation of polymer matrix constituent

To analyze the nonlinear, strain rate dependent deformation of the polymer matrix constituent, the Bodner–Partom viscoplastic state variable model (Bodner, 2002), which was originally developed to analyze the viscoplastic deformation of metals above one-half of the melting temperature, has been modified (Goldberg et al., 2003). In state variable models, a single unified strain variable is defined to represent all inelastic strains (Stouffer and Dame, 1996). Furthermore, in the state variable approach there is no defined yield stress. Inelastic strains are assumed to be present at all values of stress, the inelastic strains are just assumed to be very small in the "elastic" range of deformation. State variables, which evolve with stress and inelastic strain, are defined to represent the average effects of the deformation mechanisms.

In the modified Bodner model, the components of the inelastic strain rate tensor, $\dot{\varepsilon}^{\mathrm{I}}_{ij}$, are defined as a function of the deviatoric stress components s_{ij}, the second invariant of the deviatoric stress tensor J_2 and an isotropic state variable Z, which represents the resistance to molecular flow. The components of the inelastic strain rate are defined as follows:

$$\dot{\varepsilon}^{\mathrm{I}}_{ij} = 2D_0 \exp\left[-\frac{1}{2}\left(\frac{Z}{\sigma_{\mathrm{e}}}\right)^{2n}\right]\left(\frac{s_{ij}}{2\sqrt{J_2}} + \alpha\delta_{ij}\right), \tag{1}$$

where D_0 and n are both material constants, with D_0 representing the maximum inelastic strain rate and n controlling the rate dependence of the material. The effective stress, σ_{e}, is defined as

$$\sigma_{\mathrm{e}} = \sqrt{3J_2} + \sqrt{3}\alpha\sigma_{kk}, \tag{2}$$

where α is a state variable controlling the level of the hydrostatic stress effects and σ_{kk} is the summation of the normal stress components which equals three times the mean stress. Note that the inelastic strains need be added to the elastic strain tensor to obtain the total strains.

The evolution rate of the internal stress state variable Z and the hydrostatic stress effect state variable α are defined by the following equations:

$$\dot{Z} = q(Z_1 - Z)\dot{e}^{\mathrm{I}}_{\mathrm{e}}, \tag{3}$$

$$\dot{\alpha} = q(\alpha_1 - \alpha)\dot{e}^{\mathrm{I}}_{\mathrm{e}}, \tag{4}$$

where q is a material constant representing the "hardening" rate, and Z_1 and α_1 are material constants representing the maximum value of Z and α, respectively. The initial values of Z and α are defined by the material constants Z_0 and α_0. The term $\dot{e}^{\mathrm{I}}_{\mathrm{e}}$ in Eqs. (3) and (4) represents the effective deviatoric inelastic strain rate, which is defined as

$$\begin{aligned} \dot{e}^{\mathrm{I}}_{\mathrm{e}} &= \sqrt{\frac{2}{3}\dot{e}^{\mathrm{I}}_{ij}\dot{e}^{\mathrm{I}}_{ij}}, \\ \dot{e}^{\mathrm{I}}_{ij} &= \dot{\varepsilon}^{\mathrm{I}}_{ij} - \dot{\varepsilon}^{\mathrm{I}}_{m}\delta_{ij}, \end{aligned} \tag{5}$$

where $\dot{\varepsilon}^{\mathrm{I}}_{ij}$ are the components of the inelastic strain rate tensor $\dot{\varepsilon}^{\mathrm{I}}_{m}$ and is the mean inelastic strain rate. In many state variable constitutive models developed to analyze the behavior of metals (Stouffer and Dame, 1996), the total inelastic strain and strain rate are used in the evolution laws and are assumed to be equal to their deviatoric values. As discussed by Li and Pan (1990), since hydrostatic stresses contribute to the inelastic strains in polymers, indicating volumetric effects are present, the mean inelastic strain rate cannot be assumed to be zero, as is the case in the inelastic analysis of metals. Further information on the constitutive model, along with the procedures required to obtain the material constants, can be found in Goldberg et al. (2003).

2.2. Micromechanics model

To compute the effective strain rate dependent, nonlinear, deformation response of polymer matrix composites based on the responses of the individual constituents, a micromechanical model, which was originally proposed to analyze the in-plane deformations of fiber-reinforced composite materials, has been

modified (Kim et al., 2004). The ability to describe the transverse shear behavior, which is important in the impact problem, has been added to the modified micromechanics model.

In the modified micromechanics model, the composite laminas are assumed to have a periodic, square fiber packing and a perfect interfacial bond. The unit cell is defined to consist of a single fiber and its surrounding matrix. The unit cell is divided into several rectangular, horizontal slices of equal thickness as shown in Fig. 1. Due to symmetry, only one-quarter of the unit cell needs to be analyzed. Each slice is then separated into two subslices, one composed of fiber material and the other composed of matrix material. The fiber is assumed to be transversely isotropic, linear elastic and rate independent (common assumptions for carbon fibers) with a circular cross-section. The matrix is assumed to be an isotropic, rate dependent, inelastic material and can be characterized using the equations described in the previous section. The relations between the local strains, $\varepsilon_{ij}^{\mathrm{F}}$ and $\varepsilon_{ij}^{\mathrm{M}}$, and the local stresses, σ_{ij}^{F} and σ_{ij}^{M}, in the fiber and matrix, respectively, are described as follows:

$$\varepsilon_{ij}^{\mathrm{F}} = S_{ijkl}^{\mathrm{F}}\sigma_{kl}^{\mathrm{F}}, \quad i,j,k,l = 1,\ldots,3, \tag{6}$$

$$\varepsilon_{ij}^{\mathrm{M}} = S_{ijkl}^{\mathrm{M}}\sigma_{kl}^{\mathrm{M}} + \varepsilon_{ij}^{\mathrm{IM}}, \quad i,j,k,l = 1,\ldots,3, \tag{7}$$

where S_{ijkl}^{F} and S_{ijkl}^{M} represent the components of the compliance tensors of the fiber and matrix constituents, respectively. $\varepsilon_{ij}^{\mathrm{IM}}$ represents the inelastic strains in the matrix constituent.

The assumptions for the in-plane behavior of the unit cell are made on two levels, the slice level and the unit cell level. At the slice level, along the fiber direction (direction 1), the strains are assumed to be uniform in each subslice, and the stresses are combined using volume averaging. The in-plane transverse normal stresses (direction 2) and in-plane shear stresses (direction 12) are assumed to be uniform in each subslice, and the strains are combined using volume averaging. The out-of-plane normal strains (direction 3) are assumed to be uniform in each subslice, and the volume average of the out-of-plane stresses in each subslice is assumed to be zero. For example, for a specific slice i, these assumptions on the relationships among the stresses and strains in the fiber and matrix, $\sigma_{ij}^{i\mathrm{F}}$, $\sigma_{ij}^{i\mathrm{M}}$, $\varepsilon_{ij}^{i\mathrm{F}}$ and $\varepsilon_{ij}^{i\mathrm{M}}$, the equivalent stresses and strains of the slice, σ_{ij}^{i}, ε_{ij}^{i}, and the fiber volume fraction of the slice, V_{f}^{i}, can be expressed as follows:

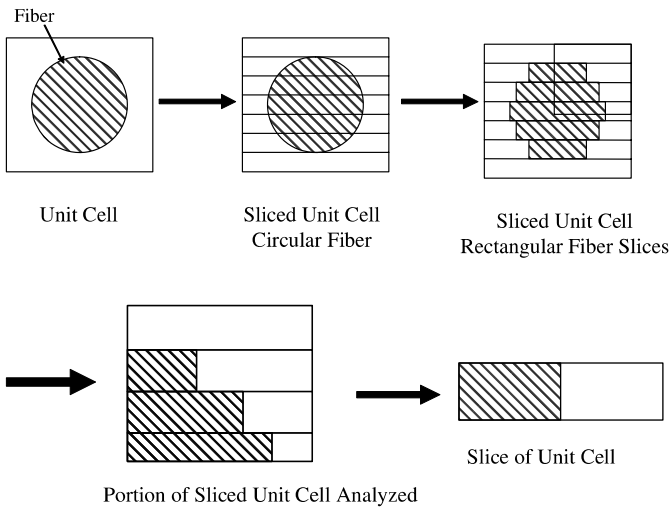

Fig. 1. Schematic showing relationship between unit cell and slices.

$$
\begin{aligned}
&\varepsilon_{11}^{i\mathrm{F}} = \varepsilon_{11}^{i\mathrm{M}} = \varepsilon_{11}^{i},\\
&\sigma_{11}^{i} = V_{\mathrm{f}}^{i}\sigma_{11}^{i\mathrm{F}} + (1 - V_{\mathrm{f}}^{i})\sigma_{11}^{i\mathrm{M}},\\
&\varepsilon_{22}^{i} = V_{\mathrm{f}}^{i}\varepsilon_{22}^{i\mathrm{F}} + (1 - V_{\mathrm{f}}^{i})\varepsilon_{22}^{i\mathrm{M}},\\
&\sigma_{22}^{i\mathrm{F}} = \sigma_{22}^{i\mathrm{M}} = \sigma_{22}^{i},\\
&\varepsilon_{12}^{i} = V_{\mathrm{f}}^{i}\varepsilon_{12}^{i\mathrm{F}} + (1 - V_{\mathrm{f}}^{i})\varepsilon_{12}^{i\mathrm{M}},\\
&\sigma_{12}^{i\mathrm{F}} = \sigma_{12}^{i\mathrm{M}} = \sigma_{12}^{i},\\
&\varepsilon_{33}^{i\mathrm{F}} = \varepsilon_{33}^{i\mathrm{M}} = \varepsilon_{33}^{i},\\
&\sigma_{33}^{i} = 0 = V_{\mathrm{f}}^{i}\sigma_{33}^{i\mathrm{F}} + (1 - V_{\mathrm{f}}^{i})\sigma_{33}^{i\mathrm{M}}.
\end{aligned}
\tag{8}
$$

On the unit cell level, the in-plane strains for each slice are assumed to be constant and equal to the equivalent in-plane strains of the unit cell. The equivalent in-plane stresses of the unit cell are computed by using volume averaging of the in-plane stresses of each slice. That is,

$$
\begin{aligned}
&\begin{Bmatrix} \varepsilon_{11} \\ \varepsilon_{22} \\ \varepsilon_{12} \end{Bmatrix} = \begin{Bmatrix} \varepsilon_{11}^{i} \\ \varepsilon_{22}^{i} \\ \varepsilon_{12}^{i} \end{Bmatrix}, \quad i = 1, \ldots, N_{\mathrm{f}} + 1,\\
&\begin{Bmatrix} \sigma_{11} \\ \sigma_{22} \\ \sigma_{12} \end{Bmatrix} = \sum_{i=1}^{N_{\mathrm{f}}+1} \begin{pmatrix} \sigma_{11}^{i} \\ \sigma_{22}^{i} \\ \sigma_{12}^{i} \end{pmatrix} h_{\mathrm{f}}^{i}
\end{aligned}
\tag{9}
$$

where σ_{ij} and ε_{ij} are the equivalent in-plane stresses and strains in the unit cell, respectively. N_{f} represents the number of fiber slices in the quarter of the unit cell which is analyzed, and h_{f}^{i} represents the ratio of the thickness of the slice i to the total thickness of the quarter of the unit cell.

Similar two-level assumptions are also proposed for the transverse shear behavior in the unit cell. Along the directions 13 (subscript 13) and 23 (subscript 23), the stresses are assumed to be uniform in each slice (and its subslices), and the strains are combined using volume averaging. That is, for the slice i, these assumptions are expressed as follows:

$$
\begin{aligned}
&\sigma_{23}^{i\mathrm{F}} = \sigma_{23}^{i\mathrm{M}} = \sigma_{23}^{i},\\
&\varepsilon_{23}^{i} = V_{\mathrm{f}}^{i}\varepsilon_{23}^{i\mathrm{F}} + (1 - V_{\mathrm{f}}^{i})\varepsilon_{23}^{i\mathrm{M}},\\
&\sigma_{13}^{i\mathrm{F}} = \sigma_{13}^{i\mathrm{M}} = \sigma_{13}^{i},\\
&\varepsilon_{13}^{i} = V_{\mathrm{f}}^{i}\varepsilon_{13}^{i\mathrm{F}} + (1 - V_{\mathrm{f}}^{i})\varepsilon_{13}^{i\mathrm{M}}.
\end{aligned}
\tag{10}
$$

At the unit cell level, along the direction 13, the strains are assumed to be uniform for all slices, and the stresses are combined using volume averaging. Along direction 23, the stresses are assumed to be uniform for all slices, and the strains are combined using volume averaging. These assumptions can be expressed using the following equations:

$$
\begin{aligned}
&\begin{Bmatrix} \sigma_{23} \\ \varepsilon_{13} \end{Bmatrix} = \begin{Bmatrix} \sigma_{23}^{i} \\ \varepsilon_{13}^{i} \end{Bmatrix}, \quad i = 1, \ldots, N_{\mathrm{f}} + 1,\\
&\begin{Bmatrix} \varepsilon_{23} \\ \sigma_{13} \end{Bmatrix} = \sum_{i=1}^{N_{\mathrm{f}}+1} \begin{Bmatrix} \varepsilon_{23}^{i} \\ \sigma_{13}^{i} \end{Bmatrix} h_{\mathrm{f}}^{i}.
\end{aligned}
\tag{11}
$$

Solving a series of equations describing the assumptions (Eqs. (8)–(11)) and the constitutive equations for the fiber and matrix (Eqs. (6) and (7)), the relationships between the equivalent stresses and the equivalent strains of the unit cell are obtained

$$\begin{Bmatrix} \sigma_{11} \\ \sigma_{22} \\ \sigma_{12} \\ \sigma_{23} \\ \sigma_{13} \end{Bmatrix} = \begin{bmatrix} Q_{11} & Q_{12} & 0 & 0 & 0 \\ & Q_{22} & 0 & 0 & 0 \\ & & Q_{66} & 0 & 0 \\ & & & Q_{23} & 0 \\ \text{sym.} & & & & Q_{55} \end{bmatrix} \begin{Bmatrix} \varepsilon_{11} - \varepsilon_{11}^{\mathrm{I}} \\ \varepsilon_{22} - \varepsilon_{22}^{\mathrm{I}} \\ \varepsilon_{12} - \varepsilon_{12}^{\mathrm{I}} \\ \varepsilon_{23} - \varepsilon_{23}^{\mathrm{I}} \\ \varepsilon_{13} - \varepsilon_{13}^{\mathrm{I}} \end{Bmatrix}, \tag{12}$$

where $\varepsilon_{ij}^{\mathrm{I}}$ represents the equivalent inelastic strains in the unit cell. Q_{ij} denotes the effective stiffness matrix of the unit cell. Detailed information on the equivalent constitutive model of the unit cell, along with the procedures to obtain $\varepsilon_{ij}^{\mathrm{I}}$ and Q_{ij} in Eq. (12) and the validation of the assumptions of the micromechanics model, can be found in Goldberg et al. (2003) and Kim et al. (2004).

The advantage of this type of modeling approach over other micromechanics methods is in reducing the complexity of the analysis and increasing the computational efficiency significantly. The in-plane behavior of each slice is decoupled, so the in-plane response of each slice can be determined independently, resulting in a series of small matrix equations instead of one large system of coupled equations. The transverse shear behavior of the unit cell can be expressed explicitly due to the simplicities of the transverse shear constitutive equations.

2.3. Verification of the micromechanics model under transverse shear loadings

Some validations of the micromechanics model have been conducted under in-plane loading conditions (Goldberg et al., 2003). The results obtained using the present micromechanics model showed a good correlation with the experimental results. However, no experimental results are currently available for the validation of the micromechanics model under transverse shear loadings. The commercial finite element software ABAQUS/Explicit (Anonymous, 2003) and alternative theoretical results were used to verify the transverse shear moduli obtained using the micromechanics model (Kim et al., 2004). In the present paper, the accuracy of the micromechanics model is further established by comparing the stress–strain curves along the 23 direction, computed using the current micromechanics model at various strain rates, with results obtained using ABAQUS (Anonymous, 2003). Previous results (Kim et al., 2004) have shown

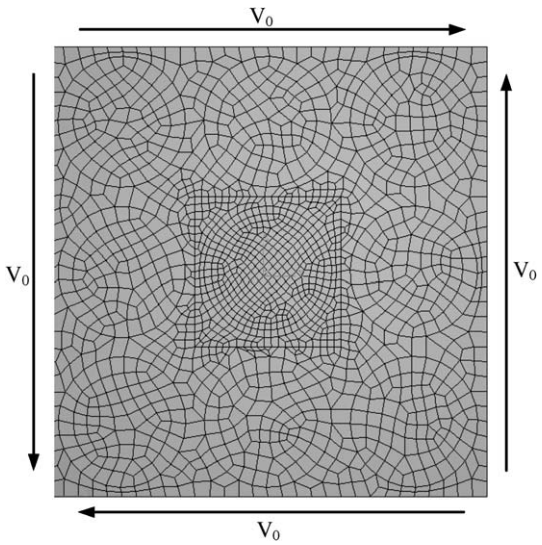

Fig. 2. Analysis model used.

that when loading is applied on an assemblage of 3×3 or more unit cells, the central unit cell undergoes a realistic deformation and the results converge. Therefore, an assemblage of 3×3 unit cells is used in the finite element model in ABAQUS(Anonymous, 2003). A velocity V_0, which is calculated from a specified strain rate, is applied to each side of the analytical model as shown in Fig. 2 (which is a very thin plate with the front and back surfaces being fixed along the out of plane direction). The equivalent stresses and strains at the central unit cell are calculated as follows:

$$\begin{aligned} \sigma_{23} &= \sum_i \sigma_{23i} V_i \Big/ \sum_i V_i, \\ \gamma_{23} &= \sum_i \gamma_{23i} V_i \Big/ \sum_i V_i, \end{aligned} \tag{13}$$

where the summation is over the elements i. The quantities V_i, σ_{23i} and γ_{23i} represent the volume of the element, the transverse shear stress and the transverse shear strain in element i, respectively. Details on the specific verification studies that were conducted can be found later in this article.

3. Finite element formulations

A micro–macro numerical procedure is developed based on the micromechanics model and HOT. Firstly, the HOT is extended to consider the inelastic deformations. The equivalent inelastic constitutive relationship for the composite laminated plate is obtained. Next, a nonlinear finite element model based on the extended HOT is developed. The nonlinear micromechanics model is then implemented into the nonlinear finite element procedure.

3.1. Refined higher order laminated plate theory

In HOT, cubic through-the-thickness variations are assumed to describe the in-plane deformations, and the out of plane deformation is assumed to be independent of the laminate thickness. The displacement field is expressed as follows:

$$\begin{aligned} u(x,y,z,t) &= u_0(x,y,t) + z\psi_{x1}(x,y,t) + z^2\psi_{x2}(x,y,t) + z^3\psi_{x3}(x,y,t), \\ v(x,y,z,t) &= v_0(x,y,t) + z\psi_{y1}(x,y,t) + z^2\psi_{y2}(x,y,t) + z^3\psi_{y3}(x,y,t), \\ w(x,y,z,t) &= w_0(x,y,t), \end{aligned} \tag{14}$$

where t is time. u, v and w are the displacements of the point (x,y,z) in the plate, and u_0, v_0 and w_0 are the corresponding values in the mid-plane. The z-coordinate is normal to the plane of the plate and measured from the mid-plane along the thickness. The quantities ψ_{x1}, ψ_{x2}, ψ_{x3}, ψ_{y1}, ψ_{y2}, and ψ_{y3} are the corresponding higher-order terms in the Taylor's series expansion. Application of the stress-free boundary conditions, $\sigma_{13}|_{z=\pm h/2} = \sigma_{23}|_{z=\pm h/2} = 0$ (where h is the total thickness of the plate), at the top and bottom surfaces, results in the simplified expression for the displacement field described in Eq. (14)

$$\begin{aligned} u &= u_0 + z\left(\psi_x - \frac{\partial w}{\partial x}\right) - \frac{4z^3}{3h^2}\psi_x, \\ v &= v_0 + z\left(\psi_y - \frac{\partial w}{\partial y}\right) - \frac{4z^3}{3h^2}\psi_y, \\ w &= w_0, \end{aligned} \tag{15}$$

where the values of ψ_x and ψ_y can be thought of as quantification of the magnitudes of transverse shear stresses present in the laminate, and zero values of the two quantities reduce the above formulation of HOT into the CLPT. The definitions of ψ_x and ψ_y can be expressed as follows:

$$\begin{aligned}\psi_x &= \psi_{x1} + \frac{\partial w}{\partial x},\\ \psi_y &= \psi_{y1} + \frac{\partial w}{\partial y}.\end{aligned} \tag{16}$$

The strains in the composite plate are then determined by differentiating the displacements described in Eq. (15), resulting in the following expressions:

$$\begin{aligned}\varepsilon_1 &= \varepsilon_1^{(0)} + z\varepsilon_1^{(1)} + z^3\varepsilon_1^{(3)},\\ \varepsilon_2 &= \varepsilon_2^{(0)} + z\varepsilon_2^{(1)} + z^3\varepsilon_2^{(3)},\\ \varepsilon_6 &= \varepsilon_6^{(0)} + z\varepsilon_6^{(1)} + z^3\varepsilon_6^{(3)},\\ \varepsilon_4 &= \varepsilon_4^{(0)} + z^2\varepsilon_4^{(2)},\\ \varepsilon_5 &= \varepsilon_5^{(0)} + z^2\varepsilon_5^{(2)},\end{aligned} \tag{17}$$

where the strains are expressed using conventional engineering notations (that is, $1 = 11$, $2 = 22$, $6 = 12$, $4 = 23$ and $5 = 13$) and

$$\begin{aligned}&\varepsilon_1^{(0)} = \frac{\partial u_0}{\partial x}, \quad \varepsilon_1^{(1)} = \frac{\partial \psi_x}{\partial x} - \frac{\partial^2 w}{\partial x^2}, \quad \varepsilon_1^{(3)} = -\frac{4}{3h^2}\frac{\partial \psi_x}{\partial x},\\ &\varepsilon_2^{(0)} = \frac{\partial v_0}{\partial y}, \quad \varepsilon_2^{(1)} = \frac{\partial \psi_y}{\partial y} - \frac{\partial^2 w}{\partial y^2}, \quad \varepsilon_2^{(3)} = -\frac{4}{3h^2}\frac{\partial \psi_y}{\partial y},\\ &\varepsilon_6^{(0)} = \frac{\partial u_0}{\partial y} + \frac{\partial v_0}{\partial x}, \quad \varepsilon_6^{(1)} = \frac{\partial \psi_x}{\partial y} + \frac{\partial \psi_y}{\partial x} - 2\frac{\partial^2 w}{\partial x \partial y}, \quad \varepsilon_6^{(3)} = -\frac{4}{3h^2}\left(\frac{\partial \psi_x}{\partial y} + \frac{\partial \psi_y}{\partial x}\right),\\ &\varepsilon_4^{(0)} = \psi_y, \quad \varepsilon_4^{(2)} = -\frac{4}{h^2}\psi_y,\\ &\varepsilon_5^{(0)} = \psi_x, \quad \varepsilon_5^{(2)} = -\frac{4}{h^2}\psi_x.\end{aligned} \tag{18}$$

For a composite laminated plate composted of several layers, the constitutive equations for each layer can be written as follows in the structural system

$$\boldsymbol{\sigma} = \overline{\mathbf{Q}}(\boldsymbol{\varepsilon} - \boldsymbol{\varepsilon}^{\mathrm{I}}), \tag{19}$$

where the stress vector $\boldsymbol{\sigma}$ the strain vector $\boldsymbol{\varepsilon}$, the inelastic strain vector $\boldsymbol{\varepsilon}^{\mathrm{I}}$ and the stiffness matrix $\overline{\mathbf{Q}}$ are all defined in the structural coordinate system and are expressed as follows:

$$\boldsymbol{\sigma} = [\,\sigma_1 \quad \sigma_2 \quad \sigma_6 \quad \sigma_4 \quad \sigma_5\,]^{\mathrm{T}}, \tag{20}$$

$$\boldsymbol{\varepsilon} = [\,\varepsilon_1 \quad \varepsilon_2 \quad \varepsilon_6 \quad \varepsilon_4 \quad \varepsilon_5\,]^{\mathrm{T}}, \tag{21}$$

$$\boldsymbol{\varepsilon}^{\mathrm{I}} = [\,\varepsilon_1^{\mathrm{I}} \quad \varepsilon_2^{\mathrm{I}} \quad \varepsilon_6^{\mathrm{I}} \quad \varepsilon_4^{\mathrm{I}} \quad \varepsilon_5^{\mathrm{I}}\,]^{\mathrm{T}}, \tag{22}$$

$$\overline{\mathbf{Q}} = \mathbf{T}\mathbf{Q}\mathbf{T}^{\mathrm{T}}, \tag{23}$$

where the superscript T represents the transpose of a vector or matrix. $\mathbf{Q}$ is the stiffness matrix of a layer in the material system as described in Eq. (12) and $\mathbf{T}$ represents the corresponding transformation tensor for the layer. Substituting Eq. (17) into Eq. (19) and integrating through all the layers in the composite plate, the following nonlinear constitutive equations for the composite laminated plate are obtained:

$$\begin{Bmatrix} \begin{Bmatrix} N_1 \\ N_2 \\ N_6 \end{Bmatrix} \\ \begin{Bmatrix} M_1 \\ M_2 \\ M_6 \end{Bmatrix} \\ \begin{Bmatrix} P_1 \\ P_2 \\ P_6 \end{Bmatrix} \end{Bmatrix} = \begin{bmatrix} \begin{bmatrix} A_{11} & A_{12} & A_{16} \\ & A_{22} & A_{26} \\ \text{sym.} & & A_{66} \end{bmatrix} & \begin{bmatrix} B_{11} & B_{12} & B_{16} \\ & B_{22} & B_{26} \\ \text{sym.} & & B_{66} \end{bmatrix} & \begin{bmatrix} E_{11} & E_{12} & E_{16} \\ & E_{22} & E_{26} \\ \text{sym.} & & E_{66} \end{bmatrix} \\ & \begin{bmatrix} D_{11} & D_{12} & D_{16} \\ & D_{22} & D_{26} \\ \text{sym.} & & D_{66} \end{bmatrix} & \begin{bmatrix} F_{11} & F_{12} & F_{16} \\ & F_{22} & F_{26} \\ \text{sym.} & & F_{66} \end{bmatrix} \\ \text{symmetric} & & \begin{bmatrix} H_{11} & H_{12} & H_{16} \\ & H_{22} & H_{26} \\ \text{sym.} & & H_{66} \end{bmatrix} \end{bmatrix} \begin{Bmatrix} \begin{Bmatrix} \varepsilon_1^{(0)} \\ \varepsilon_2^{(0)} \\ \varepsilon_6^{(0)} \end{Bmatrix} \\ \begin{Bmatrix} \varepsilon_1^{(1)} \\ \varepsilon_2^{(1)} \\ \varepsilon_6^{(1)} \end{Bmatrix} \\ \begin{Bmatrix} \varepsilon_1^{(3)} \\ \varepsilon_2^{(3)} \\ \varepsilon_6^{(3)} \end{Bmatrix} \end{Bmatrix} - \begin{Bmatrix} \begin{Bmatrix} N_1^{\mathrm{I}} \\ N_2^{\mathrm{I}} \\ N_6^{\mathrm{I}} \end{Bmatrix} \\ \begin{Bmatrix} M_1^{\mathrm{I}} \\ M_2^{\mathrm{I}} \\ M_6^{\mathrm{I}} \end{Bmatrix} \\ \begin{Bmatrix} P_1^{\mathrm{I}} \\ P_2^{\mathrm{I}} \\ P_6^{\mathrm{I}} \end{Bmatrix} \end{Bmatrix}, \tag{24}$$

$$\begin{Bmatrix} Q_4 \\ Q_5 \\ R_4 \\ R_5 \end{Bmatrix} = \begin{bmatrix} A_{44} & A_{45} & D_{44} & D_{45} \\ & A_{55} & D_{45} & D_{55} \\ & & F_{44} & F_{45} \\ \text{sym.} & & & F_{55} \end{bmatrix} \begin{Bmatrix} \varepsilon_4^{(0)} \\ \varepsilon_5^{(0)} \\ \varepsilon_4^{(2)} \\ \varepsilon_5^{(2)} \end{Bmatrix} - \begin{Bmatrix} Q_4^{\mathrm{I}} \\ Q_5^{\mathrm{I}} \\ R_4^{\mathrm{I}} \\ R_5^{\mathrm{I}} \end{Bmatrix}, \tag{25}$$

where N_i, M_i, P_i, Q_i and R_i are force and moment resultants. N_i^{I}, M_i^{I}, P_i^{I}, Q_i^{I} and R_i^{I} are inelastic force and moment resultants. A_{ij}, B_{ij}, D_{ij}, E_{ij}, F_{ij} and H_{ij} are the plate stiffness matrices. They are defined as

$$\begin{aligned} (N_i, M_i, P_i) &= \int_{-h/2}^{h/2} \sigma_i (1, z, z^3)\, \mathrm{d}z \quad (i = 1, 2, 6), \\ (Q_i, R_i) &= \int_{-h/2}^{h/2} \sigma_i (1, z^2)\, \mathrm{d}z \quad (i = 4, 5), \end{aligned} \tag{26}$$

$$\begin{aligned} (N_i^{\mathrm{I}}, M_i^{\mathrm{I}}, P_i^{\mathrm{I}}) &= \int_{-h/2}^{h/2} \overline{Q}_{ij} \varepsilon_j^{\mathrm{I}} (1, z, z^3)\, \mathrm{d}z \quad (i, j = 1, 2, 6), \\ (Q_i^{\mathrm{I}}, R_i^{\mathrm{I}}) &= \int_{-h/2}^{h/2} \overline{Q}_{ij} \varepsilon_j^{\mathrm{I}} (1, z^2)\, \mathrm{d}z \quad (i, j = 4, 5), \end{aligned} \tag{27}$$

$$\begin{aligned} (A_{ij}, B_{ij}, D_{ij}, E_{ij}, F_{ij}, H_{ij},) &= \int_{-h/2}^{h/2} \overline{Q}_{ij} (1, z, z^2, z^3, z^4, z^6)\, \mathrm{d}z \quad (i, j = 1, 2, 6), \\ (A_{ij}, D_{ij}, F_{ij}) &= \int_{-h/2}^{h/2} \overline{Q}_{ij} (1, z^2, z^4)\, \mathrm{d}z \quad (i, j = 4, 5). \end{aligned} \tag{28}$$

A more detailed description of Eqs. (24) and (25) is given in Appendix A. It should be noted that the integration between the lower and upper surfaces, $h/2$ and $-h/2$, actually involves a summation of integrations over each individual layer, since the material properties can be assumed to be different for each layer in the plate. For symmetric (about the mid-plane) plates, both B_{ij} and E_{ij} are zero.

3.2. Equation of motion

Substituting Eq. (18) into Eq. (17), the matrix form of the strain–displacement relationship can be written as

$$\boldsymbol{\varepsilon} = \mathbf{B}\mathbf{u}, \tag{29}$$

where $\mathbf{B}$ is the derivative operator matrix and the displacement vector $\mathbf{u}$ is defined as

$$\mathbf{u} = [\,u_0 \quad \psi_x \quad v_0 \quad \psi_y \quad w_0 \quad \partial w/\partial x \quad \partial w/\partial y\,]^{\mathrm{T}}. \tag{30}$$

The equation of motion can be formulated using Hamilton's Principle in a manner similar to that proposed by Tiersten (1967). The variational principle between times t_0 and t can be written as follows:

$$\delta \Pi = 0 = \int_{t_0}^{t} [\delta U + \delta W - \delta K]\, \mathrm{d}t, \tag{31}$$

where the strain energy U, the total virtual work done on the structure W and the kinetic energy K are defined as

$$\delta U = \int_S \int_{-h/2}^{h/2} \delta\boldsymbol{\varepsilon}^{\mathrm{T}}\boldsymbol{\sigma}\, \mathrm{d}z\, \mathrm{d}S = \int_S \int_{-h/2}^{h/2} \delta\boldsymbol{\varepsilon}^{\mathrm{T}}(\overline{\mathbf{Q}}(\boldsymbol{\varepsilon} - \boldsymbol{\varepsilon}^{\mathrm{I}}))\, \mathrm{d}z\, \mathrm{d}S = \int_S \int_{-h/2}^{h/2} \delta\boldsymbol{\varepsilon}^{\mathrm{T}}\overline{\mathbf{Q}}\boldsymbol{\varepsilon}\, \mathrm{d}z\, \mathrm{d}S - \int_S \int_{-h/2}^{h/2} \delta\boldsymbol{\varepsilon}^{\mathrm{T}}\overline{\mathbf{Q}}\boldsymbol{\varepsilon}^{\mathrm{I}}\, \mathrm{d}z\, \mathrm{d}S, \tag{32}$$

$$\delta W = \int_S \int_{-h/2}^{h/2} \delta\mathbf{u}^{\mathrm{T}}\mathbf{f}_{\mathbf{B}}\, \mathrm{d}z\, \mathrm{d}S + \int_S \delta\mathbf{u}^{\mathrm{T}}\mathbf{f}_{\mathbf{S}}\, \mathrm{d}S + \delta\mathbf{u}^{\mathrm{T}}\mathbf{f}_{\mathbf{P}}, \tag{33}$$

$$\delta K = \int_S \int_{-h/2}^{h/2} \rho\delta\dot{\mathbf{u}}^{\mathbf{T}}\dot{\mathbf{u}}\, \mathrm{d}z\, \mathrm{d}S, \tag{34}$$

where S is the area domain of the plate and ρ represents the mass density. The terms $\mathbf{f}_{\mathbf{B}}$, $\mathbf{f}_{\mathbf{S}}$ and $\mathbf{f}_{\mathbf{P}}$ represent body forces, surface tractions and point loads, respectively. Substituting Eqs. (23), (29), (32)–(34) into Eq. (31), the following equation of motion is obtained:

$$\int_S \int_{-h/2}^{h/2} [\delta\mathbf{u}^{\mathrm{T}}\rho\ddot{\mathbf{u}} + \delta\mathbf{u}^{\mathrm{T}}\mathbf{B}^{\mathrm{T}}\mathbf{T}\mathbf{Q}\mathbf{T}^{\mathrm{T}}\mathbf{B}\mathbf{u}]\, \mathrm{d}z\, \mathrm{d}S = \int_S \int_{-h/2}^{h/2} \delta\mathbf{u}^{\mathrm{T}}\mathbf{f}_{\mathbf{B}}\, \mathrm{d}z\, \mathrm{d}S + \int_S \delta\mathbf{u}^{\mathrm{T}}\mathbf{f}_{\mathbf{S}}\, \mathrm{d}S + \delta\mathbf{u}^{\mathrm{T}}\mathbf{f}_{\mathbf{P}} + \int_S \int_{-h/2}^{h/2} \delta\mathbf{u}^{\mathrm{T}}\mathbf{B}^{\mathrm{T}}\mathbf{T}\mathbf{Q}\mathbf{T}^{\mathrm{T}}\boldsymbol{\varepsilon}^{\mathrm{I}}\, \mathrm{d}z\, \mathrm{d}S. \tag{35}$$

3.3. Finite element discretization

In each finite element, the displacement vector described in Eq. (30) can be interpolated using the nodal displacement vector, $\mathbf{d}_{\mathbf{e}}$

$$\mathbf{u}_{\mathbf{e}} = \mathbf{N}_{\mathbf{e}}(x, y)\mathbf{d}_{\mathbf{e}}, \tag{36}$$

where $\mathbf{u}_{\mathbf{e}}$ represents the displacement vector in element $\mathbf{e}$ and $\mathbf{N}_{\mathbf{e}}(x, y)$ is the interpolation function. The finite element scheme developed in this work uses linear interpolation of the variables u, v, ψ_x and ψ_y, and a Hermite cubic polynomial function for the out of plane displacement, w. This results in seven mechanical degrees-of-freedom per node, u, v, ψ_x, ψ_y, w, $\partial w/\partial x$, and $\partial w/\partial y$. Substituting Eq. (36) into Eq. (35) and considering $\delta\mathbf{d}$ arbitrary yields the following equation:

$$\mathbf{M}\ddot{\mathbf{d}} + \mathbf{K}\mathbf{d} = \mathbf{F}_{\mathbf{1}} + \mathbf{F}_{\mathbf{2}}, \tag{37}$$

where $\mathbf{d}$ is the global nodal displacement vector. $\mathbf{M}$ is the global structural mass matrix and $\mathbf{K}$ is the global stiffness matrix. The quantities $\mathbf{F}_1$ and $\mathbf{F}_2$ represent the global force vectors due to mechanical loadings and inelastic deformations, respectively. These terms are defined as follows:

$$\begin{aligned}
\mathbf{M} &= \sum_{\mathbf{e}=1}^{n} \int_S \int_{-h/2}^{h/2} \mathbf{N}_\mathbf{e}^{\mathrm{T}} \rho \mathbf{N}_\mathbf{e} \, \mathrm{d}z \, \mathrm{d}S, \\
\mathbf{K} &= \sum_{\mathbf{e}=1}^{n} \int_S \int_{-h/2}^{h/2} \mathbf{N}_\mathbf{e}^{\mathrm{T}} \mathbf{B}^{\mathrm{T}} \mathbf{T} \mathbf{Q} \mathbf{T}^{\mathrm{T}} \mathbf{B} \mathbf{N}_\mathbf{e} \, \mathrm{d}z \, \mathrm{d}S, \\
\mathbf{F}_1 &= \sum_{\mathbf{e}=1}^{n} \left[\int_S \int_{-h/2}^{h/2} \mathbf{N}_\mathbf{e}^{\mathrm{T}} \mathbf{f}_\mathbf{B} \, \mathrm{d}z \, \mathrm{d}S + \int_S \mathbf{N}_\mathbf{e}^{\mathrm{T}} \mathbf{f}_\mathbf{S} \, \mathrm{d}S + \mathbf{N}_\mathbf{e}^{\mathrm{T}} \mathbf{f}_\mathbf{P} \right], \\
\mathbf{F}_2 &= \sum_{\mathbf{e}=1}^{n} \int_S \int_{-h/2}^{h/2} \mathbf{N}_\mathbf{e}^{\mathrm{T}} \mathbf{B}^{\mathrm{T}} \mathbf{T} \mathbf{Q} \mathbf{T}^{\mathrm{T}} \boldsymbol{\varepsilon}^{\mathrm{I}} \, \mathrm{d}z \, \mathrm{d}S,
\end{aligned} \tag{38}$$

where n is the total number of elements used in the composite plate. Four-noded rectangular isoparametric elements are used in the FEM analysis.

To solve Eq. (37), the Newmark-beta method with Newton–Raphson (NR) iteration (Argyris and Mlejnek, 1991; Bathe, 1996; Cook et al., 1989) is used in the time domain, which yields the following iterative form:

$$\overline{\mathbf{K}} \Delta \mathbf{d}^k = \mathbf{F}_1(t+\Delta t) + \mathbf{F}_2(t+\Delta t) - \mathbf{R}(t+\Delta t)^{k-1} - \mathbf{M}\mathbf{a}^{k-1}, \tag{39}$$

where k represents the iteration step. The nodal point force, $\mathbf{R}(t+\Delta t)^{(k-1)}$, which is equivalent to the elastic elemental stresses at time $(t+\Delta t)$ in the $(k-1)$th iteration, the acceleration, $\mathbf{a}^{k-1}$, and the effective stiffness matrix, $\overline{\mathbf{K}}$, are defined as follows:

$$\mathbf{R}(t+\Delta t)^{k-1} = \mathbf{K}(t+\Delta t)\mathbf{d}(t+\Delta t)^{k-1}, \tag{40}$$

$$\mathbf{a}^{k-1} = \left[\frac{4}{(\Delta t)^2} \{\mathbf{d}(t+\Delta t)^{k-1} - \mathbf{d}(t)\} - \frac{4}{\Delta t}\mathbf{v}(t) - \mathbf{a}(t) \right], \tag{41}$$

$$\overline{\mathbf{K}} = \frac{4}{(\Delta t)^2}\mathbf{M} + \mathbf{K}(t+\Delta t), \tag{42}$$

where the velocity $\mathbf{v}(t)$ and acceleration $\mathbf{a}(t)$ are obtained using the following expressions:

$$\mathbf{v}(t+\Delta t) = \{\mathbf{d}(t+\Delta t) - \mathbf{d}(t)\}\frac{2}{\Delta t} - \mathbf{v}(t), \tag{43}$$

$$\mathbf{a}(t+\Delta t) = \frac{4}{(\Delta t)^2}\{\mathbf{d}(t+\Delta t) - \mathbf{d}(t)\} - \frac{4}{\Delta t}\mathbf{v}(t) - \mathbf{a}(t). \tag{44}$$

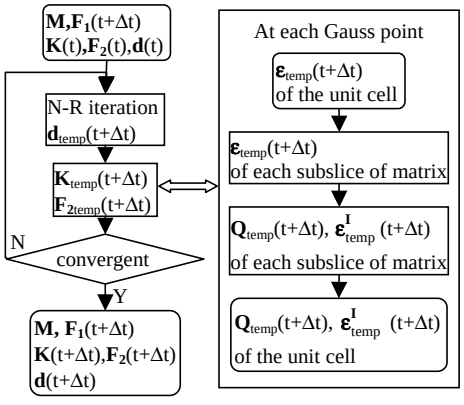

Fig. 3. Flowchart of the micro–macro numerical procedure.

3.4. Micro–macro simulation

The micromechanics model described earlier is implemented into the finite element method (FEM) to investigate the transient responses of composite laminated plates, including the effects of strain rate dependency and inelasticity. The complete flowchart of the micro–macro numerical procedure is shown in Fig. 3. Note that the global stiffness matrix, **K**, will change with the effective strain rate if the material is strain rate dependent.

4. Results and discussions

4.1. Verification of the micromechanics model

For the verification studies, properties for the representative carbon fiber-reinforced polymer matrix composite system, IM7/977-2, presented by Goldberg et al. (2003) and Goldberg (2000) are used. The material properties are listed in Table 1. The fiber is assumed to be linear elastic and the matrix is modeled using the strain rate dependent nonlinear model summarized earlier in this paper. The procedures used to determine the material constants, presented in Table 1, as well as more information about this material, are described in detail by Goldberg et al. (2003). For the matrix constituent, the variation in Young's modulus, E, as a function of the effective strain rate, $\dot{\varepsilon}$, is approximated as follows:

$$E(\dot{\varepsilon}) = \begin{cases} 6.33\ \text{GPa} & \text{for } \dot{\varepsilon} \geqslant 500, \\ 3.52 + (6.33 - 3.52)(\dot{\varepsilon} - 1.9)/(500 - 1.9)\ \text{GPa} & \text{for } 1.9 < \dot{\varepsilon} < 500, \\ 3.52\ \text{GPa} & \text{for } \dot{\varepsilon} \leqslant 1.9. \end{cases} \tag{45}$$

Details on the validation of the micromechanics model under in-plane loading conditions can be found in Goldberg et al. (2003). In conducting the validation of the micromechanics model under transverse shear loads, a fiber volume fraction of 0.6 is used in the calculation. The adequacy of the mesh size is verified via comparison of the results obtained by varying the mesh density, and 1684 8-node linear brick elements are used to mesh the thin plate in the calculation. The variation of σ_{23} with γ_{23}, computed using both the current micromechanics theory and ABAQUS finite element analyses at various strain rates, is presented in Fig. 4. It must be noted that ABAQUS results at the lowest strain rate (4.44E − 5/s) are not presented due to the extremely high computer execution time requirements. Fig. 4 shows excellent correlation between the results obtained using the current micromechanics model and those obtained using ABAQUS under both moderate and high strain rate loadings.

Table 1
Material properties of the composite material, IM7/977-2

E_{11} (GPa)		E_{22} (GPa)		G_{12} (GPa)	G_{23}(GPa)	v_{12}	v_{23}	ρ (kg/m^3)	
IM7 fibers									
276		13.8		20	5.52	0.25	0.25	1800	
$\dot{\varepsilon}$ (1/s)	E (GPa)	v	D_0 (1/s)	n	Z_0 (MPa)	Z_1 (MPa)	q	α_0	α_1	ρ (kg/m^3)
977-2 polymer matrix										
9E−5	3.52									
1.9	3.52	0.4	1.00E+06	0.8515	259.496	1131.371	150.498	0.1289	0.15215	1310
500	6.33									

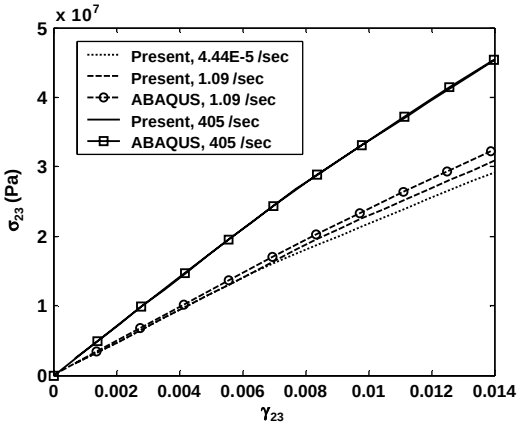

Fig. 4. Variation of σ_{23} with γ_{23}.

4.2. Transient response of the composite laminated plates

Although the developed micro–macro numerical procedure is valid for arbitrary loading conditions, in this paper, results are presented for composite plates subjected to a suddenly applied uniformly distributed loading. Square composite plates (length, $a = 0.25$ m, thickness, $h = 0.05$ m) with two different sets of material properties are considered. The first composite plate is described by using representative orthotropic, linear elastic material properties with no strain rate dependence of the elastic properties. The purpose of examining this material is to validate the basic finite element formulation without being concerned about the additional issues of nonlinearity or strain rate dependence. The next material is a representative polymer matrix composite material with a nonlinear, strain rate dependent, deformation response. By examining this material, and defining the fiber and matrix properties separately, the full capability of the matrix constitutive equations, micromechanics techniques and finite element formulation can be examined. Specifically, the material properties of the two composites are as follows:

DATA 1: $E_1 = 525$ GPa, $E_2 = E_3 = 21$ GPa, $\nu_{12} = 0.25$, $G_{12} = G_{13} = G_{23} = 10.5$ GPa, $\rho = 800$ kg/m^3 where E_i is the Young's modulus, ν_{12} is the Poisson's ratio, G_{ij} is the shear modulus and ρ represents the mass density of the composite material.

DATA 2: Composite material, IM7/977-2, with fiber volume fraction of 0.6. The material properties are presented in Table 1. The Young's modulus of the matrix constituent, E, as a function of the effective strain rate, $\dot{\varepsilon}$, is approximated as shown in Eq. (45).

To investigate the importance of using a rate dependent inelastic material model, two more simplified models for the matrix constituent of the IM7/977-2 composite are considered. These are as follows:

I. Elastic material with fixed elastic constants, that is, the value of Young's modulus is obtained from the static material test (3.52 GPa) and the effect of inelasticity is not considered.
II. Inelastic material with fixed elastic constants, that is, the value of Young's modulus is obtained from the static material test (3.52 GPa) and the effect of inelasticity, but not the effect of strain rate on the elastic properties, is considered.
III. Inelastic material with strain rate dependent elastic constants, that is, the Young's modulus is changed with the effective strain rate and the effect of inelasticity is considered.

The differences in the transient responses using these three models for the matrix constituent are further investigated under two boundary conditions.

(1) Clamped edge (CC) boundary condition: all four edges clamped, that is

$$u_0 = v_0 = w_0 = \psi_x = \psi_y = \partial w/\partial x = \partial w/\partial y = 0 \quad \text{at all the edges}$$

(2) Clamped-supported edge (CS) boundary condition: two edges clamped and two edges simply supported, that is

$$u_0 = v_0 = w_0 = \psi_x = \psi_y = \partial w/\partial x = \partial w/\partial y = 0 \quad \text{at the edges where } x = 0,\ a,$$
$$u_0 = v_0 = w_0 = 0 \quad \text{at the edges where } y = 0,\ a.$$

The applied step loading on the upper surface of the plate is expressed as follows:

$$P(t) = \begin{cases} q_0 & \text{for } t \geqslant 0, \\ 0 & \text{for } t < 0, \end{cases} \tag{46}$$

where q_0 represents the magnitude of the load and t is time.

4.3. Transient response of the anisotropic composite plate (DATA1) under uniformly distributed loading

The response of a clamped, square, orthotropic elastic composite plate (DATA1), with the stacking sequence [0/90/0], subject to a step loading with $q_0 = 1.0 \times 10^5$ N/m^2 is investigated in order to study the fundamental, transient dynamic finite element formulation. After conducting convergence studies, a mesh size of 9×9 elements and a time step of 5 μs are used in the calculations. The dynamic deflection at the center of the plate is computed over 250 μs and is compared with the results obtained using FSDT (Reddy, 1983). As shown in Fig. 5, good correlation is obtained between the HOT results and the FSDT results (thin plate). The small differences can be attributed to the differences between the two theories.

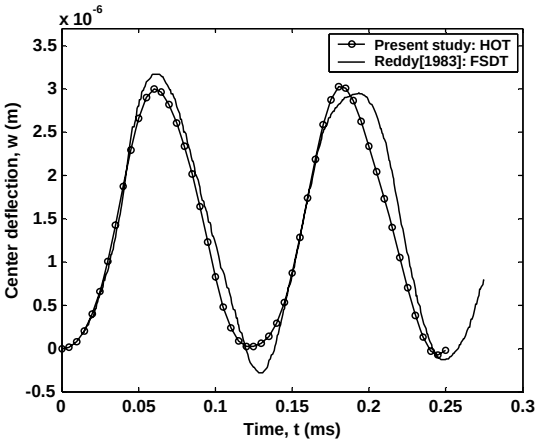

Fig. 5. Center deflection, $w(a/2, a/2)$, versus time for a [0/90/0] clamped square plate subjected to a suddenly applied loading (DATA 1, 9×9 mesh, $q_0 = 1.0 \times 10^5$ N/m^2).

4.4. Transient response of the IM7/977-2 composite plates (DATA2) using various material models

After detailed convergence studies, a 7×7 element mesh with $\Delta t = 5$ μs is used in the following computations. The transient response is obtained for a clamped composite plate with a nonlinear, strain rate dependent deformation response (DATA2) with the stacking sequence [0/90/0] subjected to a suddenly applied step loading with magnitude $q_0 = 5.0 \times 10^7$ N/m^2. The center deflection, $w(a/2, a/2)$, the center normal stresses, $\boldsymbol{\sigma}(a/2, a/2, h/2)$ and the center transverse shear stresses, $\boldsymbol{\tau}(a/2, a/2, 0)$, of the square plate, obtained using the three material models, are compared in Figs. 6–10, respectively. From Figs. 6–8, it is clear that the results obtained using models II and III indicate the presence of inelasticity due to the fact that the three curves do not lie on top of one another. Specifically, the maximum center deflection, $w_{\max}$, obtained using model I is less than that obtained using model II. However, the maximum center normal stresses, $\sigma_{x\max}$ and $\sigma_{y\max}$, obtained using model I are larger than those obtained using model II. This indicates that the model

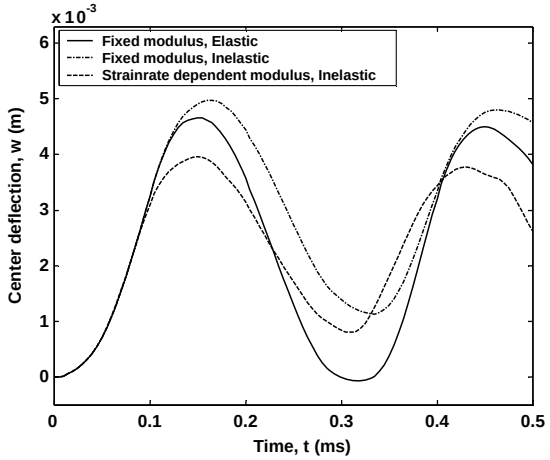

Fig. 6. Variation of center deflection, $w(a/2, a/2)$, with time for a [0/90/0] clamped square plate subjected to a suddenly applied loading (DATA 2, 7×7 mesh, $q_0 = 5.0 \times 10^7$ N/m^2).

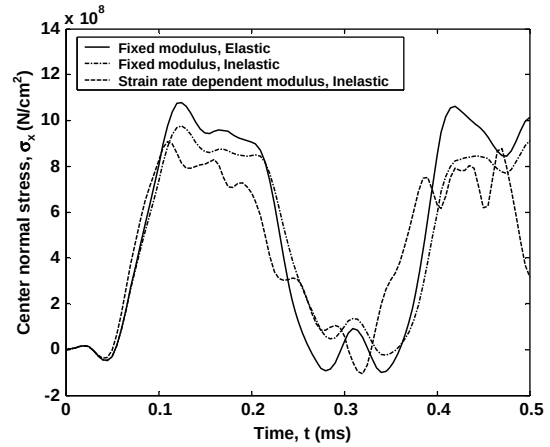

Fig. 7. Variation of center normal stress, $\sigma_x(a/2, a/2, h/2)$, with time for a [0/90/0] clamped square plate subjected to a suddenly applied loading (DATA 2, 7×7 mesh, $q_0 = 5.0 \times 10^7$ N/m^2).

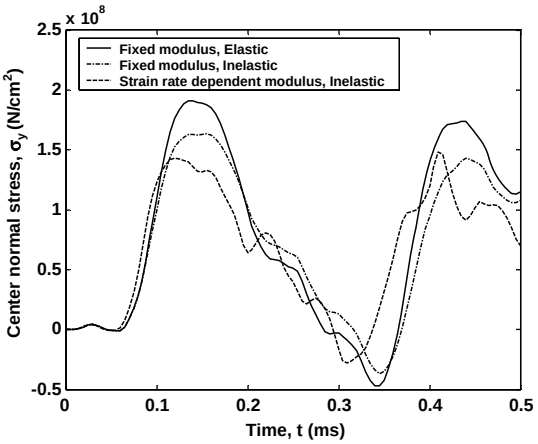

Fig. 8. Variation of center normal stress, $\sigma_y(a/2, a/2, h/2)$, with time for a [0/90/0] clamped square plate subjected to a suddenly applied loading (DATA 2, 7×7 mesh, $q_0 = 5.0 \times 10^7$ N/m^2).

including inelasticity is softer than the elastic model, which is consistent with the results obtained by Kommineni and Kant (1993). It can also be seen, from these figures, that both the maximum center deflection and the maximum center normal stresses obtained using model II are larger than those obtained using model III. This can be explained as follows. When the strain rate effect of the elastic properties of the matrix material is considered, the Young's modulus of the matrix increases with an increase in the effective strain rate. This results in a significant increase in the effective transverse shear moduli and a relatively small change in the effective Young's moduli of the composite material. Therefore, the effect of the transverse shear stresses is larger, resulting in a smaller center deflection. As a result, the center normal strain is smaller, which results in lower values of the center normal stresses. Thus, although the magnitudes of the transverse shear stresses (see Figs. 9 and 10) are much smaller, compared to the normal stresses (see Figs. 6–8), their effects cannot be ignored. The difference between results obtained using models I and III is due to the combination of the effects of inelasticity and strain rate dependency. As a result, the maximum center deflection and maximum center normal stresses are overpredicted by model I. Figs. 11 and 12 present

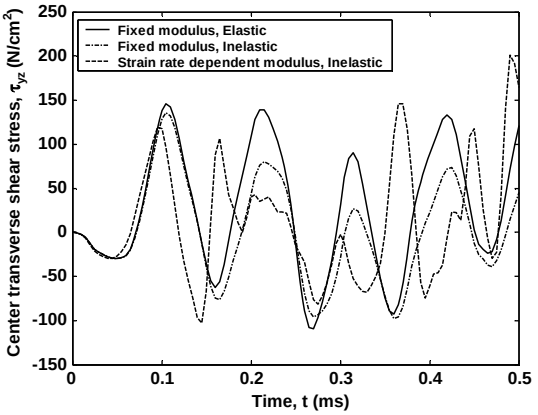

Fig. 9. Variation of center transverse shear stress, $\tau_{yz}(a/2, a/2, 0)$, with time for a [0/90/0] clamped square plate subjected to a suddenly applied loading (DATA 2, 7×7 mesh, $q_0 = 5.0 \times 10^7$ N/m^2).

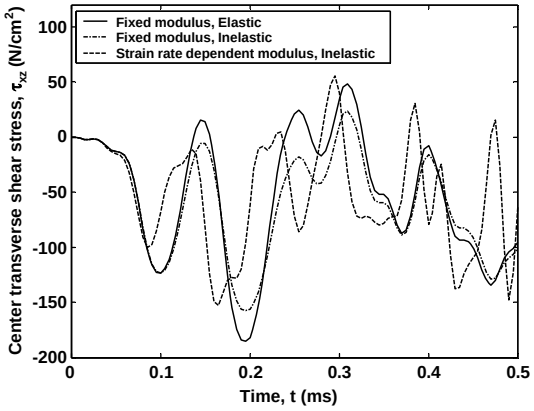

Fig. 10. Variation of center transverse shear stress, $\tau_{xz}(a/2, a/2, 0)$, with time for a [0/90/0] clamped square plate subjected to a suddenly applied loading (DATA 2, 7×7 mesh, $q_0 = 5.0 \times 10^7$ N/m^2).

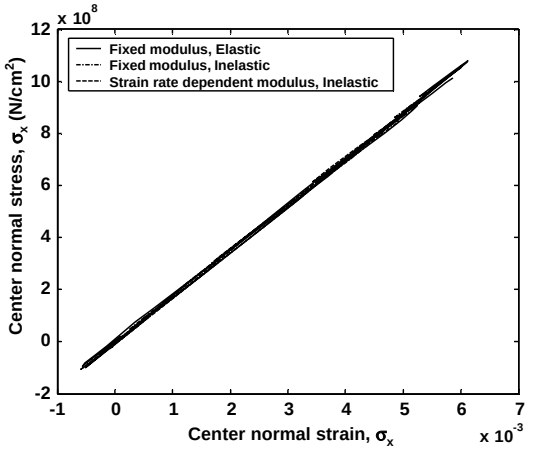

Fig. 11. Comparison of center stress–strain histories in the x direction for a [0/90/0] clamped square plate subjected to a suddenly applied loading (DATA 2, 7×7 mesh, $q_0 = 5.0 \times 10^7$ N/m^2).

the stress–strain histories of point $(a/2, a/2, h/2)$ along the x and y directions, respectively. Along the x direction, the curves obtained using all three models are almost linear. However, significant nonlinearities are observed in y direction for models II and III. This is due to the fact that for this particular laminated plate, the fiber orientation in the first layer coincides with the x axis and the matrix plays a more dominant role in the stress analysis along the y axis. However, an important point to note for this set of results and for the results discussed in the remainder of this paper is that for the plates with strain rate dependence and inelasticity present, there are currently not any experimental data or alternative theoretical calculations available with which to compare the results computed using the analysis method described here. Therefore, only qualitative, not quantitative, conclusions can be reached regarding the performance of the analysis method.

4.5. Transient response of the IM7/977-2 composite plates (DATA2) under various load magnitudes

To investigate the effects of the strain rate dependency of the matrix elastic properties and the matrix nonlinearity under different load magnitudes, a clamped three-layer composite laminated plate with the

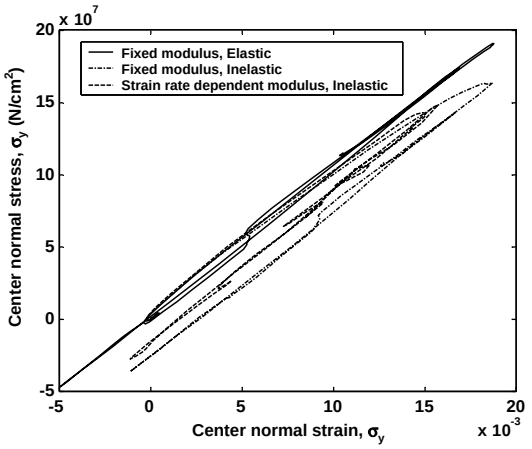

Fig. 12. Comparison of center stress–strain histories in the y direction for a [0/90/0] clamped square plate subjected to a suddenly applied loading (DATA 2, 7×7 mesh, $q_0 = 5.0 \times 10^7$ N/m^2).

stacking sequence [0/90/0] is analyzed with q_0 varying from 1.0×10^5 N/m$^2 \sim 1.0 \times 10^8$ N/m^2. Figs. 13–15 present variations of the center deflections, $w(a/2, a/2)$ and the center normal stresses, $\sigma(a/2, a/2, h/2)$, respectively, with time, obtained using model III. As seen from these figures, the variations are not proportional to the magnitude of the load due to the varying effects of the change of elastic properties with strain rate and the nonlinearity of the matrix material. The variations in the maximum center deflection and maximum center normal stresses with respect to the load magnitude are presented in Figs. 16–18 using all three matrix models (I–III). Nonlinear variations are observed when models II and III are used. Both model I and model II predict higher maximum center deflections and maximum center normal stresses as compared to Model III. Also, the differences between the models increase with an increase in the loading magnitude, which results in deformation occurring at a higher stain rate, which illustrates the significance of simulating the variation of the elastic properties with strain rate and the nonlinearity of the matrix material.

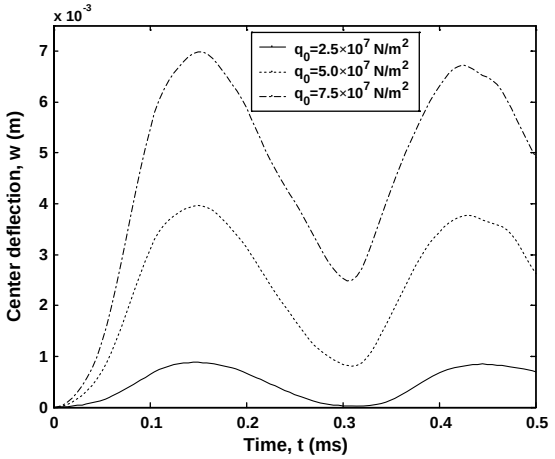

Fig. 13. Variation of center deflection, $w(a/2, a/2)$, with time for a [0/90/0] clamped square plate subjected to different load magnitudes, q_0's. (DATA 2, 7×7 mesh, model III).

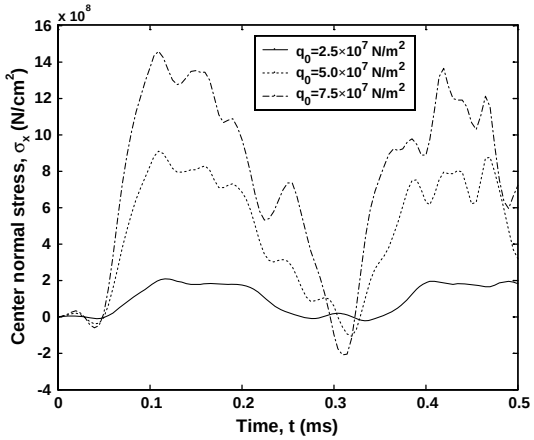

Fig. 14. Variation of center normal stresses, $\sigma_x(a/2, a/2, h/2)$, with time for a [0/90/0] clamped square plate subjected to different load magnitudes, q_0's. (DATA 2, 7×7 mesh, model III).

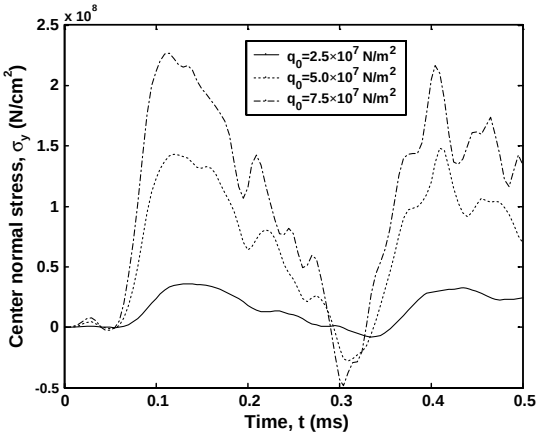

Fig. 15. Variation of center normal stresses, $\sigma_y(a/2, a/2, h/2)$, with time for a [0/90/0] clamped square plate subjected to different load magnitudes, q_0's. (DATA 2, 7×7 mesh, model III).

4.6. Transient response of the IM7/977-2 composite plates (DATA2) under various boundary conditions

Results are presented for composite plates, with the stacking sequence [0/90/0], subjected to a suddenly applied step loading of magnitude $q_0 = 5.0 \times 10^7$ N/m^2. Two different boundary conditions, clamped edges (CC) and clamped-supported edges (CS), are used. The transient responses, shown in Fig. 19, are calculated using matrix model III. The results show that the maximum center deflection and the residual deformation (represented by the point with the second minimum deflection in the curve) obtained using the CS boundary condition are larger than those obtained using the CC boundary condition. This implies that inelastic strain effects are increased for the plate with the CS boundary condition. The maximum center values (center deflections and center normal stresses) under both the CC and CS boundary conditions, as well the differences of these values under the CC and CS boundary conditions, are presented in Table 2. The column denoted *Err* represents the boundary influence and is represented using the following expression:

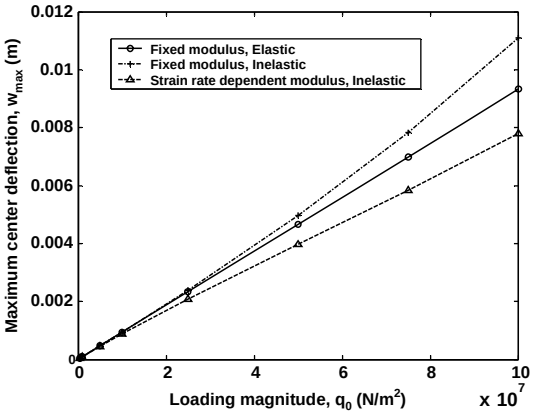

Fig. 16. Comparison of maximum center deflection, $w_{\max}(a/2, a/2)$, with load magnitude, q_0, for a [0/90/0] clamped square plate subjected to suddenly applied loading (DATA 2, 7×7 mesh).

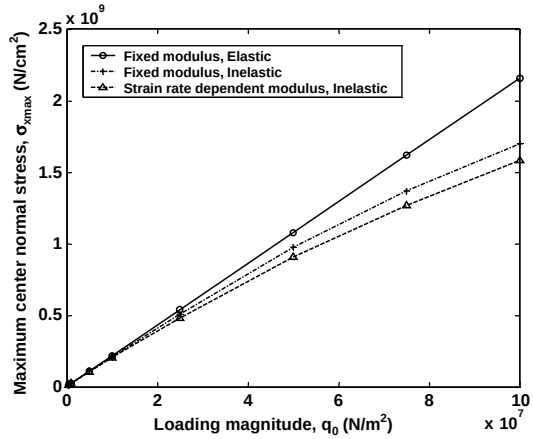

Fig. 17. Comparison of maximum center normal stresses, $\sigma_{x\max}(a/2, a/2, h/2)$, with load magnitude, q_0, for a [0/90/0] clamped square plate subjected to a suddenly applied loading (DATA 2, 7×7 mesh).

$$z_{\mathrm{Err}} = (z_{\mathrm{CS}} - z_{\mathrm{CC}})/[\tfrac{1}{2}(z_{\mathrm{CS}} + z_{\mathrm{CC}})], \tag{47}$$

where z represents one of the maximum center values, $w_{\max}$, $\sigma_{x\max}$ and $\sigma_{y\max}$. The subscripts Err, CS and CC are the names of the columns where the value of z is obtained. Comparing the z_{Err}'s obtained using the different matrix models, it can be concluded that the effect of the matrix model on the influence of the boundary conditions is reasonably small.

4.7. Transient response of the IM7/977-2 composite plates (DATA2) with various stacking sequences

To investigate the influence of the stacking sequence on the maximum center deflection, composite plates subjected to a suddenly applied step loading with magnitude $q_0 = 5.0 \times 10^7$ N/m^2 are investigated. The

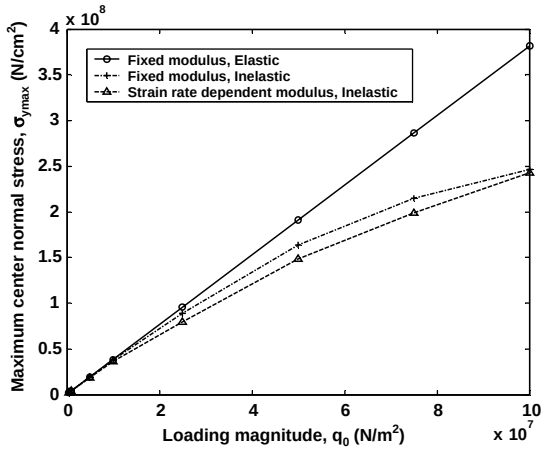

Fig. 18. Comparison of maximum center normal stresses, $\sigma_{y\max}(a/2, a/2, h/2)$, with load magnitude, q_0, for a [0/90/0] clamped square plate subjected to a suddenly applied loading (DATA 2, 7×7 mesh).

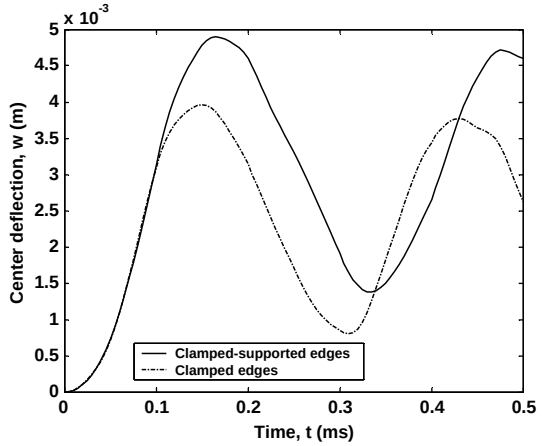

Fig. 19. Variation of center deflection, $w(a/2, a/2)$, with time for a [0/90/0] clamped square plate subjected to suddenly applied loading under different boundary conditions (DATA 2, 7×7 mesh).

Table 2
Comparisons of maximum center values under different boundary conditions

Model	$w_{\max}(a/2, a/2)$, (10^{-3} m)			$\sigma_{x\max}(a/2, a/2, h/2)$ (GPa)			$\sigma_{y\max}(a/2, a/2, h/2)$ (GPa)		
	CC	CS	Err	CC	CS	Err	CC	CS	Err
I	4.6601	5.7482	0.2091	1.0791	1.3334	0.2108	0.1892	0.1908	0.0084
II	4.9749	6.3525	0.2432	0.9772	1.1658	0.1760	0.1734	0.1744	0.0058
III	3.9646	4.8983	0.2107	0.9085	1.1090	0.1987	0.1482	0.1485	0.0020

stacking sequence of the composite plate is $[\alpha/(\alpha + \beta/\alpha]$, as shown in Fig. 20. Four cases of ply variation are used to investigate the effect of anisotropy.

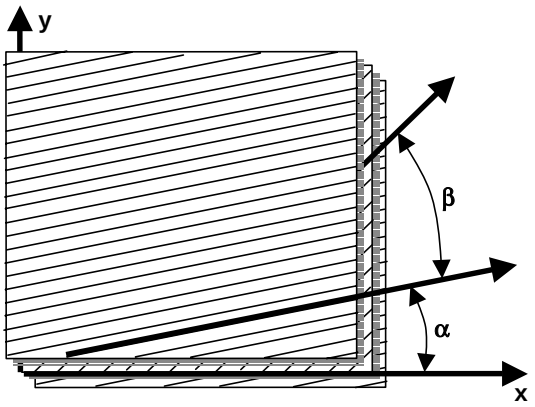

Fig. 20. Schematic showing of composite stacking sequence.

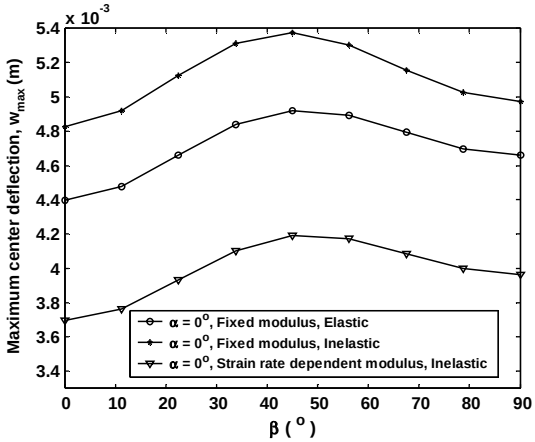

Fig. 21. Variation of maximum center deflection, $w_{\max}(a/2, a/2)$, with stacking sequence under CC boundary condition.

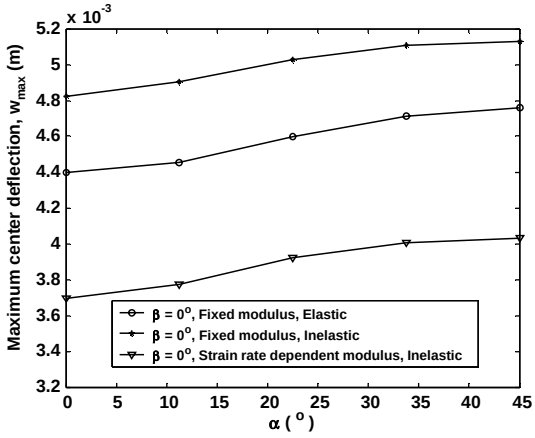

Fig. 22. Variation of maximum center deflection, $w_{\max}(a/2, a/2)$, with stacking sequence under CC boundary condition.

Case A: Under clamped edges (CC) boundary condition, the range of β is 0–90° and α is 0°.
Case B: Under clamped edges (CC) boundary condition, the range of α is 0–45° and β is 0°.
Case C: Under clamped-supported edges (CS) boundary condition, the range of β is 0–90° and α is 0°.
Case D: Under clamped-supported edges (CS) boundary condition, the range of α is 0–45° and β is 0°.

The variations of the maximum center deflection with stacking sequence for cases A–D are presented in Figs. 21–24, respectively. It can be observed that the influence of stacking sequence on the maximum center deflection obtained using the three models of the matrix constituent is similar. Comparing Figs. 21 and 23, it is clear that, under both CC and CS boundary conditions, the maximum center deflection increases at the beginning ($\beta < 45°$) and then decreases ($45° < \beta < 90°$) with an increase in the value of β. However, the results shown in Figs. 22 and 24 indicate that the maximum center deflection increases ($\alpha < 45°$) with an increase in the value of α under both CC and CS boundary conditions. This is due to the fact that, in these cases, the ply with fiber orientation of 45° is most flexible.

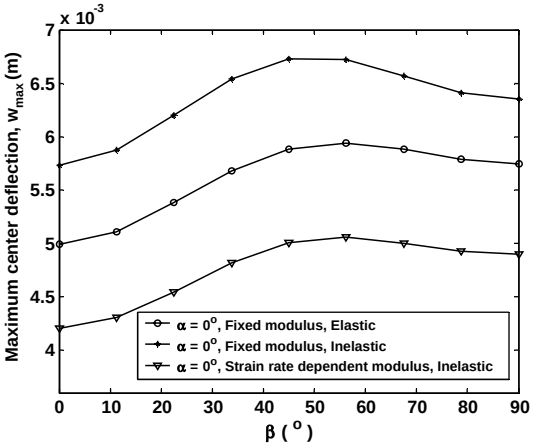

Fig. 23. Variation of maximum center deflection, $w_{\max}(a/2, a/2)$, with stacking sequence under CS boundary condition.

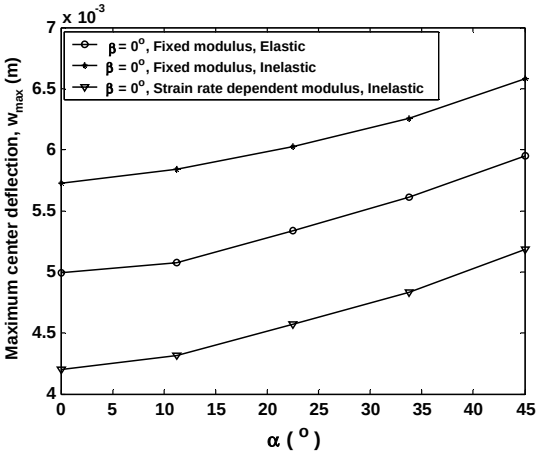

Fig. 24. Variation of maximum center deflection, $w_{\max}(a/2, a/2)$, with stacking sequence under CS boundary condition.

5. Conclusions

A multiscale numerical procedure is developed to accurately model a strain rate dependent, inelastic composite plate. A micromechanics model, which accounts for the transverse shear stress effect, the effects of strain rate, and the effects of matrix inelasticity is used for accurate and efficient analysis of the mechanical responses of the fiber and matrix constituents. The accuracy of the micromechanics model under transverse shear loads has been verified. A HOT is extended to accurately capture the inelastic deformations of the composite plate. The mathematical model is implemented using the finite element technique. The developed procedure is used to investigate the transient responses of composite plates subjected to suddenly applied loadings. The results are compared using different models for the matrix constituent of the composite, under various boundary conditions, subjected to step loadings with various magnitudes, and for composite plates with various stacking sequences. The following important observations are made from the present study.

1. Excellent agreement is found between the transverse shear stress–strain curves obtained using the micromechanics model and those obtained using ABAQUS under both moderate and high strain rate loadings.
2. Excellent agreement is observed in the variation of center displacement with time between the result obtained using the present HOT model and that in the literature.
3. The maximum center deflection obtained using an elastic model for the matrix is less than that obtained using an inelastic model for the matrix. However, the maximum center normal stresses obtained using the matrix elastic model is larger than those obtained using an inelastic model for the matrix. Both the maximum center deflection and the maximum center normal stresses obtained using models where the matrix elastic properties do not vary with strain rate(both elastic and inelastic model) are larger than those obtained using a model where the matrix elastic properties are allowed to vary with strain rate.
4. The stress–strain curves show significant nonlinearities in the direction normal to the fiber direction using both models incorporating inelasticity in the matrix constituent.
5. The differences between the results obtained using different models increase with an increase in the load magnitude.
6. The influences of boundary condition on the maximum center deflection and normal stresses obtained using all three matrix models are similar.
7. The influence of ply stacking sequence on the maximum center deflection is similar for both Clamped-clamped (CC) and Clamped-supported (CS) boundary conditions. The trends are similar for all three matrix models considered. The maximum center deflection is obtained when α and β are equal to 45°.

Acknowledgments

The authors acknowledge the support of NASA Glenn Research Center, Grant No. NCC3-1024, technical monitor, Robert K. Goldberg, in conducting this research.

Appendix A

Expressions for force and moment resultants N_i, M_i, P_i $(i = 1,2,6)$ and Q_i, R_i $(i = 4,5)$ in Eqs. (24) and (25) are as follows:

$$
\begin{aligned}
N_i &= \int_{-h/2}^{h/2} \sigma_i \,\mathrm{d}z = \int_{-h/2}^{h/2} [\overline{Q}_{i1}(\varepsilon_1 - \varepsilon_1^{\mathrm{I}}) + \overline{Q}_{i2}(\varepsilon_2 - \varepsilon_2^{\mathrm{I}}) + \overline{Q}_{i6}(\varepsilon_6 - \varepsilon_6^{\mathrm{I}})] \,\mathrm{d}z \\
&= \int_{-h/2}^{h/2} (\overline{Q}_{i1}\varepsilon_1 + \overline{Q}_{i2}\varepsilon_2 + \overline{Q}_{i6}\varepsilon_6) \,\mathrm{d}z - \int_{-h/2}^{h/2} (\overline{Q}_{i1}\varepsilon_1^{\mathrm{I}} + \overline{Q}_{i2}\varepsilon_2^{\mathrm{I}} + \overline{Q}_{i6}\varepsilon_6^{\mathrm{I}}) \,\mathrm{d}z \\
&= \int_{-h/2}^{h/2} [\overline{Q}_{i1}(\varepsilon_1^{(0)} + z\varepsilon_1^{(1)} + z^3\varepsilon_1^{(3)}) + \overline{Q}_{i2}(\varepsilon_2^{(0)} + z\varepsilon_2^{(1)} + z^3\varepsilon_2^{(3)}) + \overline{Q}_{i6}(\varepsilon_6^{(0)} + z\varepsilon_6^{(1)} + z^3\varepsilon_6^{(3)})] \,\mathrm{d}z \\
&\quad - \int_{-h/2}^{h/2} (\overline{Q}_{i1}\varepsilon_1^{\mathrm{I}} + \overline{Q}_{i2}\varepsilon_2^{\mathrm{I}} + \overline{Q}_{i6}\varepsilon_6^{\mathrm{I}}) \,\mathrm{d}z \\
&= \left(\int_{-h/2}^{h/2} \overline{Q}_{i1} \,\mathrm{d}z\varepsilon_1^{(0)} + \int_{-h/2}^{h/2} \overline{Q}_{i2} \,\mathrm{d}z\varepsilon_2^{(0)} + \int_{-h/2}^{h/2} \overline{Q}_{i6} \,\mathrm{d}z\varepsilon_6^{(0)} \right) \\
&\quad + \left(\int_{-h/2}^{h/2} \overline{Q}_{i1} z \,\mathrm{d}z\varepsilon_1^{(1)} + \int_{-h/2}^{h/2} \overline{Q}_{i2} z \,\mathrm{d}z\varepsilon_2^{(1)} + \int_{-h/2}^{h/2} \overline{Q}_{i6} z \,\mathrm{d}z\varepsilon_6^{(1)} \right) \\
&\quad + \left(\int_{-h/2}^{h/2} \overline{Q}_{i1} z^3 \,\mathrm{d}z\varepsilon_1^{(3)} + \int_{-h/2}^{h/2} \overline{Q}_{i2} z^3 \,\mathrm{d}z\varepsilon_2^{(3)} + \int_{-h/2}^{h/2} \overline{Q}_{i6} z^3 \,\mathrm{d}z\varepsilon_6^{(3)} \right) \\
&\quad - \int_{-h/2}^{h/2} (\overline{Q}_{i1}\varepsilon_1^{\mathrm{I}} + \overline{Q}_{i2}\varepsilon_2^{\mathrm{I}} + \overline{Q}_{i6}\varepsilon_6^{\mathrm{I}}) \,\mathrm{d}z
\end{aligned}
$$

$$
\begin{aligned}
M_i &= \int_{-h/2}^{h/2} \sigma_i z \,\mathrm{d}z = \int_{-h/2}^{h/2} [\overline{Q}_{i1}(\varepsilon_1 - \varepsilon_1^{\mathrm{I}}) + \overline{Q}_{i2}(\varepsilon_2 - \varepsilon_2^{\mathrm{I}}) + \overline{Q}_{i6}(\varepsilon_6 - \varepsilon_6^{\mathrm{I}})] z \,\mathrm{d}z \\
&= \int_{-h/2}^{h/2} (\overline{Q}_{i1}\varepsilon_1 + \overline{Q}_{i2}\varepsilon_2 + \overline{Q}_{i6}\varepsilon_6) z \,\mathrm{d}z - \int_{-h/2}^{h/2} (\overline{Q}_{i1}\varepsilon_1^{\mathrm{I}} + \overline{Q}_{i2}\varepsilon_2^{\mathrm{I}} + \overline{Q}_{i6}\varepsilon_6^{\mathrm{I}}) z \,\mathrm{d}z \\
&= \int_{-h/2}^{h/2} [\overline{Q}_{i1}(\varepsilon_1^{(0)} + z\varepsilon_1^{(1)} + z^3\varepsilon_1^{(3)}) + \overline{Q}_{i2}(\varepsilon_2^{(0)} + z\varepsilon_2^{(1)} + z^3\varepsilon_2^{(3)}) + \overline{Q}_{i6}(\varepsilon_6^{(0)} + z\varepsilon_6^{(1)} + z^3\varepsilon_6^{(3)})] z \,\mathrm{d}z \\
&\quad - \int_{-h/2}^{h/2} (\overline{Q}_{i1}\varepsilon_1^{\mathrm{I}} + \overline{Q}_{i2}\varepsilon_2^{\mathrm{I}} + \overline{Q}_{i6}\varepsilon_6^{\mathrm{I}}) z \,\mathrm{d}z \\
&= \left(\int_{-h/2}^{h/2} \overline{Q}_{i1} z \,\mathrm{d}z\varepsilon_1^{(0)} + \int_{-h/2}^{h/2} \overline{Q}_{i2} z \,\mathrm{d}z\varepsilon_2^{(0)} + \int_{-h/2}^{h/2} \overline{Q}_{i6} z \,\mathrm{d}z\varepsilon_6^{(0)} \right) \\
&\quad + \left(\int_{-h/2}^{h/2} \overline{Q}_{i1} z^2 \,\mathrm{d}z\varepsilon_1^{(1)} + \int_{-h/2}^{h/2} \overline{Q}_{i2} z^2 \,\mathrm{d}z\varepsilon_2^{(1)} + \int_{-h/2}^{h/2} \overline{Q}_{i6} z^2 \,\mathrm{d}z\varepsilon_6^{(1)} \right) \\
&\quad + \left(\int_{-h/2}^{h/2} \overline{Q}_{i1} z^4 \,\mathrm{d}z\varepsilon_1^{(3)} + \int_{-h/2}^{h/2} \overline{Q}_{i2} z^4 \,\mathrm{d}z\varepsilon_2^{(3)} + \int_{-h/2}^{h/2} \overline{Q}_{i6} z^4 \,\mathrm{d}z\varepsilon_6^{(3)} \right) \\
&\quad - \int_{-h/2}^{h/2} (\overline{Q}_{i1}\varepsilon_1^{\mathrm{I}} + \overline{Q}_{i2}\varepsilon_2^{\mathrm{I}} + \overline{Q}_{i6}\varepsilon_6^{\mathrm{I}}) z \,\mathrm{d}z
\end{aligned}
$$

$$
\begin{aligned}
P_i &= \int_{-h/2}^{h/2} \sigma_i z^3 \,\mathrm{d}z = \int_{-h/2}^{h/2} [\overline{Q}_{i1}(\varepsilon_1 - \varepsilon_1^{\mathrm{I}}) + \overline{Q}_{i2}(\varepsilon_2 - \varepsilon_2^{\mathrm{I}}) + \overline{Q}_{i6}(\varepsilon_6 - \varepsilon_6^{\mathrm{I}})] z^3 \,\mathrm{d}z \\
&= \int_{-h/2}^{h/2} (\overline{Q}_{i1}\varepsilon_1 + \overline{Q}_{i2}\varepsilon_2 + \overline{Q}_{i6}\varepsilon_6) z^3 \,\mathrm{d}z - \int_{-h/2}^{h/2} (\overline{Q}_{i1}\varepsilon_1^{\mathrm{I}} + \overline{Q}_{i2}\varepsilon_2^{\mathrm{I}} + \overline{Q}_{i6}\varepsilon_6^{\mathrm{I}}) z^3 \,\mathrm{d}z \\
&= \int_{-h/2}^{h/2} [\overline{Q}_{i1}(\varepsilon_1^{(0)} + z\varepsilon_1^{(1)} + z^3\varepsilon_1^{(3)}) + \overline{Q}_{i2}(\varepsilon_2^{(0)} + z\varepsilon_2^{(1)} + z^3\varepsilon_2^{(3)}) + \overline{Q}_{i6}(\varepsilon_6^{(0)} + z\varepsilon_6^{(1)} + z^3\varepsilon_6^{(3)})] z^3 \,\mathrm{d}z \\
&\quad - \int_{-h/2}^{h/2} (\overline{Q}_{i1}\varepsilon_1^{\mathrm{I}} + \overline{Q}_{i2}\varepsilon_2^{\mathrm{I}} + \overline{Q}_{i6}\varepsilon_6^{\mathrm{I}}) z^3 \,\mathrm{d}z = \left(\int_{-h/2}^{h/2} \overline{Q}_{i1} z^3 \,\mathrm{d}z\varepsilon_1^{(0)} + \int_{-h/2}^{h/2} \overline{Q}_{i2} z^3 \,\mathrm{d}z\varepsilon_2^{(0)} + \int_{-h/2}^{h/2} \overline{Q}_{i6} z^3 \,\mathrm{d}z\varepsilon_6^{(0)} \right) \\
&\quad + \left(\int_{-h/2}^{h/2} \overline{Q}_{i1} z^4 \,\mathrm{d}z\varepsilon_1^{(1)} + \int_{-h/2}^{h/2} \overline{Q}_{i2} z^4 \,\mathrm{d}z\varepsilon_2^{(1)} + \int_{-h/2}^{h/2} \overline{Q}_{i6} z^4 \,\mathrm{d}z\varepsilon_6^{(1)} \right) \\
&\quad + \left(\int_{-h/2}^{h/2} \overline{Q}_{i1} z^6 \,\mathrm{d}z\varepsilon_1^{(3)} + \int_{-h/2}^{h/2} \overline{Q}_{i2} z^6 \,\mathrm{d}z\varepsilon_2^{(3)} + \int_{-h/2}^{h/2} \overline{Q}_{i6} z^6 \,\mathrm{d}z\varepsilon_6^{(3)} \right) \\
&\quad - \int_{-h/2}^{h/2} (\overline{Q}_{i1}\varepsilon_1^{\mathrm{I}} + \overline{Q}_{i2}\varepsilon_2^{\mathrm{I}} + \overline{Q}_{i6}\varepsilon_6^{\mathrm{I}}) z^3 \,\mathrm{d}z
\end{aligned}
$$

$$
\begin{aligned}
Q_i &= \int_{-h/2}^{h/2} \sigma_i \,\mathrm{d}z = \int_{-h/2}^{h/2} [\overline{Q}_{i4}(\varepsilon_4 - \varepsilon_4^{\mathrm{I}}) + \overline{Q}_{i5}(\varepsilon_5 - \varepsilon_5^{\mathrm{I}})] \,\mathrm{d}z \\
&= \int_{-h/2}^{h/2} (\overline{Q}_{i4}\varepsilon_4 + \overline{Q}_{i5}\varepsilon_5) \,\mathrm{d}z - \int_{-h/2}^{h/2} (\overline{Q}_{i4}\varepsilon_4^{\mathrm{I}} + \overline{Q}_{i5}\varepsilon_5^{\mathrm{I}}) \,\mathrm{d}z \\
&= \int_{-h/2}^{h/2} [\overline{Q}_{i4}(\varepsilon_4^{(0)} + z^2\varepsilon_4^{(2)}) + \overline{Q}_{i5}(\varepsilon_5^{(0)} + z^2\varepsilon_5^{(2)})] \,\mathrm{d}z - \int_{-h/2}^{h/2} (\overline{Q}_{i4}\varepsilon_4^{\mathrm{I}} + \overline{Q}_{i5}\varepsilon_5^{\mathrm{I}}) \,\mathrm{d}z \\
&= \left(\int_{-h/2}^{h/2} \overline{Q}_{i4} \,\mathrm{d}z\varepsilon_4^{(0)} + \int_{-h/2}^{h/2} \overline{Q}_{i5} \,\mathrm{d}z\varepsilon_5^{(0)} \right) + \left(\int_{-h/2}^{h/2} \overline{Q}_{i4} z^2 \,\mathrm{d}z\varepsilon_4^{(2)} + \int_{-h/2}^{h/2} \overline{Q}_{i5} z^2 \,\mathrm{d}z\varepsilon_5^{(2)} \right) \\
&\quad - \int_{-h/2}^{h/2} (\overline{Q}_{i4}\varepsilon_4^{\mathrm{I}} + \overline{Q}_{i5}\varepsilon_5^{\mathrm{I}}) \,\mathrm{d}z
\end{aligned}
$$

$$
\begin{aligned}
R_i &= \int_{-h/2}^{h/2} \sigma_i z^2 \,\mathrm{d}z = \int_{-h/2}^{h/2} [\overline{Q}_{i4}(\varepsilon_4 - \varepsilon_4^{\mathrm{I}}) + \overline{Q}_{i5}(\varepsilon_5 - \varepsilon_5^{\mathrm{I}})] z^2 \,\mathrm{d}z \\
&= \int_{-h/2}^{h/2} (\overline{Q}_{i4}\varepsilon_4 + \overline{Q}_{i5}\varepsilon_5) z^2 \,\mathrm{d}z - \int_{-h/2}^{h/2} (\overline{Q}_{i4}\varepsilon_4^{\mathrm{I}} + \overline{Q}_{i5}\varepsilon_5^{\mathrm{I}}) z^2 \,\mathrm{d}z \\
&= \int_{-h/2}^{h/2} [\overline{Q}_{i4}(\varepsilon_4^{(0)} + z^2\varepsilon_4^{(2)}) + \overline{Q}_{i5}(\varepsilon_5^{(0)} + z^2\varepsilon_5^{(2)})] z^2 \,\mathrm{d}z - \int_{-h/2}^{h/2} (\overline{Q}_{i4}\varepsilon_4^{\mathrm{I}} + \overline{Q}_{i5}\varepsilon_5^{\mathrm{I}}) z^2 \,\mathrm{d}z \\
&= \left(\int_{-h/2}^{h/2} \overline{Q}_{i4} z^2 \,\mathrm{d}z\varepsilon_4^{(0)} + \int_{-h/2}^{h/2} \overline{Q}_{i5} z^2 \,\mathrm{d}z\varepsilon_5^{(0)} \right) + \left(\int_{-h/2}^{h/2} \overline{Q}_{i4} z^4 \,\mathrm{d}z\varepsilon_4^{(2)} + \int_{-h/2}^{h/2} \overline{Q}_{i5} z^4 \,\mathrm{d}z\varepsilon_5^{(2)} \right) \\
&\quad - \int_{-h/2}^{h/2} (\overline{Q}_{i4}\varepsilon_4^{\mathrm{I}} + \overline{Q}_{i5}\varepsilon_5^{\mathrm{I}}) z^2 \,\mathrm{d}z
\end{aligned}
$$

References

Aboudi, J.A., 1989. Micromechanical analysis of composites by the method of cells. Applied Mechanics Review 42, 193–221.

Anonymous, ABAQUS/Explicit Users Manual, Version 6.4, ABAQUS, Inc., Pawtucket, RI, 2003.

Argyris, J., Mlejnek, H.P., 1991Dynamics of Structures. Text on Computational Mechanics, vol. 5. Elsevier Science Publishers.

Bathe, K.J., 1996. Finite Element Procedures. Prentice-Hall, Englewood Cliffs, NJ.

Bodner, S.R., 2002. Unified Plasticity for Engineering Applications. Kluwer Academic/Plenum Publishers, New York.

Chattopadhyay, A., Gu, H., 1994. New higher-order plate theory in modeling delamination buckling of composite laminates. AIAA Journal 32 (8), 1709–1716.

Chow, T.S., 1971. On the propagation of flexural waves in anorthotropic laminated plate and its response to an impulsive load. Journal of Composite Materials 5, 306–319.

Cook, R.D., Malkus, D.S., Plesha, M.E., 1989. Concepts and Applications of Finite Element Analysis, third ed. Wiley, NY.

Flugge, W., 1967. Stresses in Shells. Springer-Verlag, New York.

Goldberg, R.K., 2000. Implementation of Laminate Theory Into Strain Rate Dependent Micromechanics Analysis of Polymer Matrix Composites, NASA/TM-2000-210351, National Aeronautics and Space Administration, Washington, DC.

Goldberg, R.K., Roberts, G.D., Gilat, A., 2003. Implementation of an Associative Flow Rule Including Hydrostatic Stress Effects Into the High Strain Rate Deformation Analysis of Polymer Matrix Composites, NASA/TM-2003-212382, National Aeronautics and Space Administration, Washington, DC.

Goldberg, R.K., Roberts, G.D., Gilat, A., 2004. Analytical studies of the high rate tensile response of a polymer matrix composite. Journal of Advanced Materials 36 (3), 14–24.

Kant, T., Khare, R.K., 1994. Finite-element thermal-stress analysis of composite laminates using a higher-order theory. Journal of Thermal Stresses 17 (2), 229–255.

Kant, T., Mallikarjuna, 1991. Nonlinear dynamics of laminated plates with a higher-order theory and Co finite-elements. International Journal of Non-Linear Mechanics 26 (3–4), 335–343.

Kant, T., Ravichandran, R.V., Pandya, B.N., et al., 1988. Finite-element transient dynamic analysis of isotropic and fiber reinforced composite plates using a higher-order theory. Composite Structures 9 (4), 319–342.

Kant, T., Varaiya, J.H., Arora, C.P., 1990. Finite-element transient analysis of composite and sandwich plates based on a refined theory and implicit time integration schemes. Computers & Structures 36 (3), 401–420.

Kant, T., Arora, C.P., Varaiya, J.H., 1992. Finite-element transient analysis of composite and sandwich plates based on a refined theory and a mode superposition method. Composite Structures 22 (2), 109–120.

Kapania, R.K., Raciti, S., 1989. Recent advances in analysis of laminated beams and plates: Part I: Shear effects and buckling. AIAA Journal 27 (7), 923–934.

Khdeir, A.A., Reddy, J.N., 1991. Thermal stresses and deflections of cross-ply laminated plates using refined plate theories. Journal of Thermal Stresses 14 (4), 419–438.

Khdeir, A.A., Rajab, M.D., Reddy, J.N., 1992. Thermal effects on the response of cross-ply laminated shallow shells. International Journal of Solids and Structures 29 (5), 653–667.

Kim, H.S., Zhu, L.F., Chattopadhyay, A., Goldberg, R.K., 2004. Implementation of Higher Order Laminate Theory Into Strain Rate Dependent Micromechanics Analysis of Polymer Matrix Composites, 45th AIAA/ASME/ASCE/AHS/ASC Structures, Structural Dynamics & Materials Conference, Palm Springs, CA, April 19–22.

Kommineni, J.R., Kant, T., 1993. Large deflection elastic and inelastic transient analyses of composite and sandwich plates with a refined theory. Journal of Reinforced Plastics and Composites 12 (11), 1150–1170.

Li, F.Z., Pan, J., 1990. Plane-stress crack-tip fields for pressure-sensitive dilatant materials. Journal of Applied Mechanics 57, 40–49.

Mallikarjuna, Kant, T., 1990. Finite-element transient-response of composite and sandwich plates with a refined higher-order theory. Journal of Applied Mechanics-Transactions of the ASME 57 (4), 1084–1086.

Mallikarjuna, Kant, T., 1993. A critical review and some results of recently developed refined theories of fiber-reinforced laminated composites and sandwiches. Composite Structures 23 (4), 293–312.

Mital, S.K., Murthy, P.L.N., Chamis, C., 1995. Micromechanics for ceramic matrix composites via fiber substructuring. Journal of Composite Materials 29, 614–633.

Noor, A.K., Burton, W.S., 1989. Assessment of shear deformation theories for multilayered composite plates. Applied Mechanics Reviews 42 (1), 1–13.

Pao, Y.C., 1972. On higher-order theory for thermoelastic analysis of heterogeneous orthotropic cylindrical shells. In: Proceedings of Southern, Conference on Theoretical and Applied Mechanics, 6th Tampa, FL, March 23, 24 (1972), University of South Florida, 1972, pp. 787–806.

Pindera, M.J., Bednarcyk, B.A., 1999. An efficient implementation of the generalized method of cells for unidirectional, multi-phased composites with complex microstructures. Composites: Part B 30, 87–105.

Reddy, J.N., 1982. On the solutions to forced response of rectangular composite plates. Journal of Applied Mechanics 49, 403–408.

Reddy, J.N., 1983. Dynamic (transient) analysis of layered anisotropic composite material plates. International Journal for Numerical Methods in Engineering 19, 237–255.
Reddy, J.N., 1984. A simple higher-order theory for laminated composite plates. Journal of Applied Mechanics 51 (4), 745–752.
Reddy, J.N., 1990. A review of refined theories of composite laminates. Shock and Vibration Digest 22, 3–17.
Reddy, J.N., 1997. Mechanics of Laminated Composite Plates: Theory and Analysis. CRC Press, Boca Raton.
Robertson, D.D., Mall, S., 1993. Micromechanical relations for fiber-reinforced composites using the free transverse shear approach. Journal of Composites Technology and Research 15, 181–192.
Stouffer, D.C., Dame, L.T., 1996. Inelastic Deformation of Metals. Models, Mechanical Properties and Metallurgy. John Wiley and Sons, New York.
Sun, C.T., Chen, J.L., 1991. A micromechanics model for plastic behavior of fibrous composites. Composites Science and Technology 40, 115–129.
Tiersten, H.F., 1967. Hamilton's principle for linear piezoelectric media. IEEE Proceedings 55 (8), 1523–1524.
Varadan, T.K., Bhaskar, K., 1997. Review of different laminate theories for the analysis of composite. Journal of Aeronautics Society of India 49, 202–208.
Wang, A.S.D., Rose, J.L., Chou, P.C., 1972. Strongly coupled stress waves in heterogeneous plates. AIAA Journal 10 (8), 1088–1090.
Whitney, J.M., 1969. The effect of transverse shear deformation in the bending of laminated plates. Journal of Composite Materials 3, 534–547.
Whitney, J.M., 1993. A laminate analogy for micromechanics. In: Newaz, G.M. (Ed.), Proceedings of the American Society for Composites Eighth Technical Conference. Technomic Publishing Co., Lancaster, PA, pp. 785–794.